Remote Sensing of Environment 293 (2023) 113612

Contents lists available at ScienceDirect

Remote Sensing of Environment

journal homepage: www.elsevier.com/locate/rse

Mapping foliar photosynthetic capacity in sub-tropical and tropical forests with UAS-based imaging spectroscopy: Scaling from leaf to canopy

Shuwen Liu [a], Zhengbing Yan [a,b,*], Zhihui Wang [c], Shawn Serbin [d], Marco Visser [e], Yuan Zeng [f,g], Youngryel Ryu [h], Yanjun Su [g,i], Zhengfei Guo [a], Guangqin Song [a], Qianhan Wu [a], He Zhang [a], K.H. Cheng [a], Jinlong Dong [j], Billy Chi Hang Hau [a], Ping Zhao [k], Xi Yang [l], Lingli Liu [g,i], Alistair Rogers [d], Jin Wu [a,m,*]

[a] *Research Area of Ecology and Biodiversity, School of Biological Sciences, The University of Hong Kong, Pokfulam, Hong Kong, China*
[b] *State Key Laboratory of Vegetation and Environmental Change, Institute of Botany, Chinese Academy of Sciences, Xiangshan, Beijing 100093, China*
[c] *Guangdong Provincial Key Laboratory of Remote Sensing and Geographical Information System, Guangdong Open Laboratory of Geospatial Information Technology and Application, Guangzhou Institute of Geography, Guangdong Academy of Sciences, Guangzhou, China*
[d] *Environmental and Climate Sciences Department, Brookhaven National Laboratory, Upton, New York, USA*
[e] *Institute of Environmental Sciences, Leiden University, Einsteinweg 2, 2333 CC Leiden, the Netherlands*
[f] *State Key Laboratory of Remote Sensing Science, Aerospace Information Research Institute, Chinese Academy of Sciences, Beijing 100101, China*
[g] *University of Chinese Academy of Sciences, Beijing 100049, China*
[h] *Department of Landscape Architecture and Rural Systems Engineering, Seoul National University, Seoul, South Korea*
[i] *State Key Laboratory of Vegetation and Environmental Change, Institute of Botany, Chinese Academy of Sciences, Beijing, China*
[j] *CAS Key Laboratory of Tropical Forest Ecology, Xishuangbanna Tropical Botanical Garden, Chinese Academy of Sciences, Menglun, Mengla, Yunnan 666303, China*
[k] *Key Laboratory of Vegetation Restoration and Management of Degraded Ecosystems, South China Botanical Garden, Chinese Academy of Sciences, Guangzhou 510650, China*
[l] *Department of Environmental Sciences, University of Virginia, Charlottesville, VA 22903, USA*
[m] *Institute of Climate and Carbon Neutrality, The University of Hong Kong, Pokfulam, Hong Kong, China*

ARTICLE INFO

Keywords:
Photosynthetic capacity
Imaging spectroscopy
Carbon science
Individual tree crown
Leaf to canopy scaling
Canopy radiative transfer model
Plant functional traits

ABSTRACT

Accurate understanding of the variability in foliar physiological traits across landscapes is critical to improve parameterization and evaluation of terrestrial biosphere models (TBMs) that seek to represent the response of terrestrial ecosystems to a changing climate. Numerous studies suggest imaging spectroscopy can characterize foliar biochemical and morphological traits at the canopy scale, but there is only limited evidence for retrieving canopy photosynthetic capacity (e.g., maximum carboxylation rate, $V_{c,max}$ and maximum electron transport rate, J_{max}). Moreover, the effect of canopy structure within forest communities on scaling up spectra-trait relationships from leaf to canopy level is not well known. To advance the spectra-trait approach and enable the estimation of key traits using remote sensing, we collected imaging spectroscopy data from an Unoccupied Aerial System (UAS) platform over two forest sites in China (a subtropical forest in Mt. Dinghu and a tropical rainforest in Xishuangbanna). At these sites, we also collected ground measurements of leaf spectra and traits, including biochemical (leaf nitrogen, phosphorus, chlorophyll, and water content), morphological (leaf mass per area, LMA) and physiological ($V_{c,max25}$ and J_{max25}) traits ($n = 135$ tree-crowns from 42 species across two sites). Using a partial least-squares regression (PLSR) approach, we built and tested spectra-trait models with repeated cross-validation. The spectral models developed with leaf spectra were directly transferred to canopy spectra to evaluate the effect of canopy structure. We further applied canopy spectral models to map these traits at individual tree-crown scale. The results demonstrate that (1) UAS-based canopy spectra can be used to estimate $V_{c,max}$ ($R^2 = 0.55$, nRMSE = 11.79%), J_{max} ($R^2 = 0.54$, nRMSE = 12.34%), and five additional foliar traits ($R^2 = 0.38$–0.60, nRMSE = 10.11–13.56%) at the tree-crown scale with demonstrated generalizability across two sites; (2) canopy structure strongly affects the spectra-trait relationships from leaf to canopy level, but the effects vary considerably across foliar traits and cannot be well captured by the 4SAIL canopy radiative transfer model. UAS-based imaging spectroscopy maps large variability in all foliar traits (including physiological traits) with spatially explicit information, reproducing the field-observed inter- and intra-specific variations. These results

* Corresponding authors at: School of Biological Sciences, The University of Hong Kong, Pokfulam Road, Hong Kong, China.
E-mail addresses: yanzhengbing@pku.edu.cn (Z. Yan), jinwu@hku.hk (J. Wu).

https://doi.org/10.1016/j.rse.2023.113612
Received 21 November 2022; Received in revised form 19 April 2023; Accepted 30 April 2023
Available online 5 May 2023

demonstrate the capability of using UAS-based imaging spectroscopy for characterizing the variability of foliar physiological traits at individual tree-crown scale over forest landscapes and highlight the similar generalizability but different biophysical mechanisms underlying spectra-trait relationships at leaf and canopy levels.

1. Introduction

Projecting the fate of terrestrial ecosystems under climate change requires an accurate representation of carbon dioxide assimilation in terrestrial biosphere models (TBMs). Photosynthesis is the largest carbon flux between the biosphere and atmosphere (Ryu et al., 2019; Mengoli et al., 2022), and is the gatekeeper process for an uncertain terrestrial carbon sink thus playing a major role in regulating the atmospheric CO_2 level and determining the rate of global climate change (Bonan and Doney, 2018; Rogers et al., 2017; Walker et al., 2021). Accurate model projection of photosynthesis and many other key model outputs, is highly dependent upon parameterization associated with foliar photosynthetic capacity, i.e., the maximum carboxylation rate of the enzyme Rubisco and the maximum rate of electron transport standardized to a reference temperature of 25 °C ($V_{c,max25}$ and J_{max25}, respectively; Farquhar et al., 1980; Rogers et al., 2017; Ricciuto et al., 2018). These physiological traits are represented in TBMs with just 5–15 values that typically are not modified by the many biotic and abiotic processes that result in diverse and dynamic traits in nature (e.g., Kattge et al., 2009; Walker et al., 2014; Ali et al., 2015; Smith and Dukes, 2018; Wu et al., 2019; Yan et al., 2021). Advancing the ability to measure these key traits across scales from individual organisms to forest ecosystems thus represent an essential research need, which would help to improve the understanding and modelling of terrestrial carbon cycling and the response of the terrestrial biosphere to global environmental changes (Rogers et al., 2017; Bonan and Doney, 2018).

Leaf-level gas exchange is the most widely-used approach for deriving $V_{c,max25}$ and J_{max25}. This method fits field-measured photosynthetic CO_2 response curves to a biochemical photosynthesis model (Farquhar et al., 1980; Bernacchi et al., 2013), and has been used as the primary method for estimating $V_{c,max25}$ and J_{max25}. However, it is very slow, and often takes over 45 min for each single measurement (Bernacchi et al., 2003; Long, 2003). In recent years, a few faster methods of estimating $V_{c,max25}$ and J_{max25} have been proposed, such as the one point method (De Kauwe et al., 2016; Burnett et al., 2019) and the rapid A–C_i response method (Stinziano et al., 2017). However, these gas exchange measurements remain challenging in natural ecosystems and remote regions, such as subtropical and tropical forests where high species richness and tall trees would co-occur over large landscapes (Albert et al., 2018; Lamour et al., 2021; Yan et al., 2021). Canopy access presents another critical challenge in these ecosystems where canopy cranes or tree climbing strategies are needed but may be prohibitively expensive or time-consuming. The difficulties associated with sampling and measuring $V_{c,max25}$ and J_{max25}, together with the high degree of plant functional diversity in terrestrial ecosystems, make the spatial coverage of these two physiological traits woefully inadequate (Jetz et al., 2016; Kattge et al., 2020). Therefore, an alternative and rapid estimation method of $V_{c,max25}$ and J_{max25} is required, especially when considering tall trees in natural forest ecosystems and remote regions, including subtropical and tropical forests.

Recent advances in vegetation spectroscopy offer a promising alternative for efficient characterization of foliar traits from leaf to canopy levels. The approach relies upon the tight connection of leaf or canopy reflectance spectra to morphological, biochemical and physiological properties (Curran, 1989; Elvidge, 1990; Kokaly et al., 2009; Ollinger, 2011; Serbin and Townsend, 2020). Leaf spectroscopy has been used to infer a broad suite of leaf traits, including leaf morphological (e.g., leaf mass per area (LMA)), biochemical (e.g., water, chlorophyll, nitrogen, and phosphorous) and physiological traits (e.g., $V_{c,max25}$ and J_{max25}) with demonstrated high accuracy (Asner and Martin, 2008; Doughty et al., 2017; Féret et al., 2019; Serbin et al., 2014; Yan et al., 2021). Indeed leaf-level spectra-trait relationships have been shown to have a broader-scale generalizability, and a single spectral model for each trait can be developed and used across a wide spatial and temporal extent (Chen et al., 2022; Lamour et al., 2021; Martin et al., 2008; Nakaji et al., 2019; Serbin et al., 2019; Wu et al., 2019). Consistent with leaf-level studies is the demonstrated high accuracy and broad-scale generalizability of the use of the spectra-trait approach to characterizing various foliar morphological and biochemical traits via imaging spectroscopy (Asner et al., 2015; Asner and Martin, 2008; Serbin et al., 2015; Thomson et al., 2021; Townsend et al., 2003; Wang et al., 2020; Wessman et al., 1988; Zhao et al., 2018). However, the ability of scaling from leaf to canopy levels with confidence has rarely been evaluated for photosynthetic traits like $V_{c,max}$, with a few exceptions (e.g., Serbin et al., 2015; Croft et al., 2017; Fu et al., 2020; Meacham-Hensold et al., 2020) but these examples are commonly managed ecosystems with homogeneous canopy structure or based on additional trait-trait assumptions (e.g., chlorophyll-$V_{c,max}$ relationships as used in Croft et al., 2017).

Theoretically, canopy spectral variability is directly connected to leaf spectra and canopy structure, such as leaf area index and leaf angle distribution (Asner, 1998; Ollinger, 2011; Stovall et al., 2021). Therefore, despite mounting evidence showing the effectiveness of using imaging spectroscopy for characterizing foliar morphological and biochemical traits at the canopy level (e.g., Wessman et al., 1988; Asner et al., 2015; Singh et al., 2015; Wang et al., 2020), divergent agreements remain with the mechanisms underlying how canopy structure shapes canopy-level spectra-trait relationships. The spectral signal is different at the leaf and canopy level, but some traits may leave distinguishable fingerprints at both levels. For example, many earlier studies analyzed spectra-trait relationships at both leaf and canopy levels, and identified many shared and common spectral domains for trait prediction across the two levels (Baret et al., 1994; Kupiec and Curran, 1995; Dawson et al., 1999; Serrano et al., 2002). However, there remain studies demonstrating that canopy structure significantly contributes to canopy reflectance spectra and dominates canopy level spectra-trait relationships (Asner and Martin, 2008; Knyazikhin et al., 2013; le Maire et al., 2008). Fundamentally, there are two factors influencing whether the fingerprints of traits are conserved across leaf and canopy levels. Firstly, it depends on the trait, as different foliar morphological and biochemical properties are expressed differently across spectra (Kokaly et al., 2009; Ustin et al., 2009). Secondly, it depends on the spectral region since different spectral regions are affected differently by canopy structure and multiple scattering (Asner, 1998; Verrelst et al., 2015; Wang et al., 2017). However, it is still lacking a comprehensive assessment of how canopy structure influences the relationship between spectra and traits, particularly in the case of photosynthetic traits.

The goal of this study was to explore the capability, across-site generalizability, and effects of canopy structure on the cross-level (from leaf to canopy) spectra-traits relationship for characterizing foliar photosynthetic capacity in natural forest landscapes using the imaging spectroscopy approach. Towards this goal, we collected imaging spectroscopy data from an Unoccupied Aerial System (UAS) platform over two forest sites in China, in which we also collected paired ground measurements of leaf spectra and traits. With these data, we addressed the following two questions: (1) Can UAS-based imaging spectroscopy be used to estimate the variability in $V_{c,max25}$ and J_{max25} at tree-crown scale across different forest sites? (2) To what extent does canopy structure alter the cross-level spectra-trait relationship? Furthermore, can the commonly used canopy radiative transfer model PROSAIL

capture the effects of canopy structure? Afterwards, we built a workflow for applying canopy spectral models to UAS hyperspectral imagery for mapping foliar trait at individual tree-crown scale.

2. Materials and methods

2.1. Study sites

This study was conducted at two sites in Southern China, approximately 1200 km apart, including a subtropical forest at Mountain Dinghu (DH; 23°10'N, 112°32'E) and a tropical rainforest at Xishuangbanna (XSBN; 21°47' N, 101°03' E) (Fig. 1). These sites were selected because they each contained a canopy crane, operated by the Chinese Academy of Sciences, which provided access to the upper tree canopy over a 1-ha area around the tower footprint. The mean annual temperature (MAT) and precipitation (MAP) were reasonably similar between the two sites, with a MAT and MAP of 20.9 °C and 1927 mm yr^{-1}, respectively, at DH and 21.8 °C and 1493 mm yr^{-1} at XSBN (Shen et al., 2018; Ye et al., 2008). Both sites had similar laterite soil (Cao et al., 2006; Gui et al., 2019). The abundant canopy tree species representative of each site includes *Machilus breviflora*, *Castanopsis chinensis*, *Pinus massoniana*, *Schima superba* and other interspersed evergreen broad-leaved species at DH (Gui et al., 2019; Ye et al., 2008); and *Semecarpus reticulate*, *Sloanea tomentosa*, *Pometia tomentosa*, *Canarium album*, *Parashorea chinensis*, and other interspersed evergreen broad-leaves species at XSBN (Cao et al., 2006; Shen et al., 2018).

2.2. Materials

Across the two sites, intensive field campaigns were conducted in 2021 during the early growing season (April 2– April 16 at XSBN and April 22–May 5 at DH). For each selected canopy tree, only the upper canopy, sunlit foliage was sampled for measurements of leaf gas exchange, foliar reflectance and five other functional traits (i.e., leaf mass per area-LMA, leaf water content-LWC, area-based leaf nitrogen content-N_{area}, area-based leaf phosphorus content-P_{area}, and leaf chlorophyll content-Chl). We sampled these traits because they are of interest to the broader plant ecology community and are also important parameters in current ecosystem models (Bonan and Doney, 2018; Ricciuto et al., 2018; Wright et al., 2004). For each individual tree, the measurements of all sampled mature-green foliage were averaged to represent the traits of that individual (i.e., the canopy-level traits). For each tree we recorded the crown shape and coordinates with a differential GPS receiver (i90 IMU-RTK GNSS; Shanghai Huace Navigation Technology Ltd., Shanghai, China).

2.2.1. Field measurements of leaf gas exchange, spectra, and morphological and biochemical traits

Leaf gas exchange was measured using four portable gas exchange systems (LI-6400-02B LED light source and Li-6800-02 small LED light source; Li-COR Inc., Lincoln, NE, USA). The percentage use of LiCOR-6400 and 6800 was 66.4% (n = 285 leaves) and 33.6% (n = 144 leaves) in our data records, respectively. The detailed protocol of leaf gas exchange measurements and associated retrieval of $V_{c,max25}$ and J_{max25} is shown in Method S1, and summarized here. Following best practices, branches were harvested before dawn and cut under water to avoid inducing xylem embolism (Wu et al., 2019). Representative leaves (according to the colour, size and rigidity of the leaves; Chavana-Bryant et al., 2017; Wu et al., 2019) were then selected to measure the response of net CO_2 assimilation rate (A) to intracellular CO_2 concentration (C_i) (commonly known as an A-C_i curve, Bernacchi et al., 2013, e.g., Fig. S1), closely following the protocol of Yan et al. (2021). For each tree, we sampled two branches, and selected two to four leaves per branch to measure the A-C_i response.

Immediately after gas exchange measurements, we collected leaf reflectance spectra with a field-portable spectroradiometer, a Spectra Vista Corporation (SVC) HR-1024i together with their Leaf-Clip Reflectance-Probe (LC-RP-Pro) fore-optic (SVC, Poughkeepsie, NY, USA). The spectroradiometer has a full spectral range of 350–2500 nm, the full-width half maximum (FWHM) ≤3.3 nm at 700 nm, ≤9.5 nm at 1500 nm, and ≤ 6.5 nm at 2100 nm, and a final sampling internal of 1 nm through the linear interpolation (Ely et al., 2019; Yan et al., 2021).

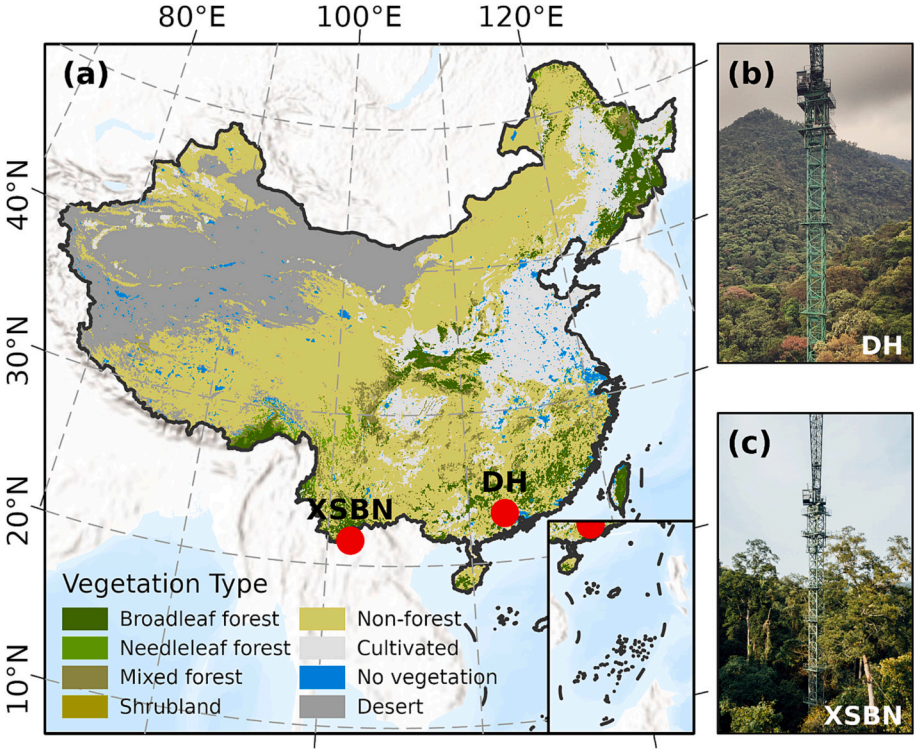

Fig. 1. Sampling sites across the two forest types in China. (a) Location of the two canopy crane sites in China, including a subtropical forest in Mountain Dinghu (DH) and a tropical rainforest in Xishuangbanna (XSBN). The background shows a map of vegetation types reclassified from the MODIS Land Cover Climate Modelling Grid Product (MCD12C1) in 2020. (b-c) At each site, the Chinese Academy of Sciences (CAS) maintains a canopy crane facility enabling access to a 1-ha area of each forest, with the crane tower height of 60 m in DH and 81 m in XSBN.

Following the protocol of Yan et al. (2021), an internal tungsten halogen lamp in the leaf reflectance probe was used to illuminate the leaf samples upon a black background, accompanied by a 99% reflective Spectralon white panel (Labsphere Inc., North Dutton, NH, USA) for the reference standard. To avoid the influence of excessive heat loads on the measured leaf reflectance spectra, we set the integral scanning time for each spectrum to 1 s with the automatic integration optimization of the SVC spectroradiometer (Serbin et al., 2019; Yan et al., 2021). Meanwhile, the Vendor-provided SVC instrument software was used to correct discontinuities in reflectance spectra within the detector overlap regions (Yan et al., 2021). For each leaf, 3–6 different parts of the leaf adaxial surface depending on leaf size were chosen to measure the reflectance spectra with one spectrum per part, and then the averaged spectra were calculated to denote the spectral properties of that leaf. Some example demonstrations for the measured leaf reflectance spectra were provided in Fig. S2.

Immediately following spectral measurements, the leaves were measured for five biochemical and morphological traits, Chl, LWC, LMA, N_{area} and P_{area}, following standard protocols. Leaf Chl content was measured by a portable optical chlorophyll meter (SPAD-502 Plus; Konika-Minolta, Inc., Tokyo, Japan) and denoted as SPAD-based leaf Chl content (Chl_{SPAD}), as the Chl_{SPAD} value has been demonstrated as a good approximate of leaf Chl content in both crops and woody plants previously (Coste et al., 2010; Silva-Perez et al., 2018; Uddling et al., 2007). After the Chl measurement, we determined leaf fresh mass using a precision balance (precision at 0.001 g; Meilen; Meifu Electronics Co. Ltd., Shenzhen, China), and then scanned each leaf with a digital scanner (CanoScan LiDE300; Canon, Tokyo, Japan) to derive leaf area using the ImageJ software (version 1.53) following Guo et al. (2022). Scanned leaves were oven-dried to constant mass at 65 °C. We then determined the LWC ($g\ g^{-1}$) from the difference between leaf fresh mass and leaf dry mass divided by leaf fresh mass. The LMA ($g\ m^{-2}$) was calculated using leaf dry mass divided by leaf area. To measure leaf N and P concentrations, dried leaves were ground with a ball mill (NM200, Retsch, Haan, Germany). Mass-based leaf N concentration was then determined with an elemental analyser (Elementar vario EL III, Elementar, Hanau, Germany; Jones, 2001) through the Dumas combustion method, and mass-based leaf P concentration was determined by inductively coupled plasma optical emission spectroscopy (Thermo 6300; Thermo Scientific, West Palm Beach, FL) after HNO_3–HF–$HClO_4$ digestion (Jones, 2001). N_{area} ($g\ m^{-2}$) and P_{area} ($g\ m^{-2}$) were then calculated using mass-based leaf N ($mg\ g^{-1}$) and P ($mg\ g^{-1}$) concentrations multiplied by LMA. We use area-based measurements because the canopy-scale radiative transfer processes depend on area-based biochemical components (Kattenborn et al., 2019) and biochemical traits are usually expressed on an area basis in terrestrial biosphere modelling studies, in line with the main function of leaves for light interception (Osnas et al., 2013; Walker et al., 2014).

2.2.2. UAS-based hyperspectral, LiDAR and RGB imagery, and data processing

The hyperspectral imagery was collected using a hyperspectral snapshot imager (ULTRIS X20 Plus; Cubert GmbH, Ulm, Baden-Württemberg, Germany). This sensor captures hyperspectral imagery with a field of view of 35°, providing 164 spectral bands over a wavelength range of 350–1000 nm with a spectral resolution of 4 nm, while the noisy segments at wavelengths below 502 nm and beyond 870 nm were later removed during data processing. As a result, 93 spectral bands covering 502–870 nm remained and were used in the later spectral analysis. The imager was installed on an UAS (DJI Matrice 300 RTK, DJI, Shenzhen, China), and used to capture the imagery of two forest sites during the same period as the field campaigns. Imagery was acquired on April 8, 2021 at XSBN and April 29, 2021 at DH. The UAS operations were carried out under clear sky conditions at around local solar noon. Each UAS flight lasted <30 min, and thus the solar angle change effect on canopy reflectance measurements would be small (Fig. S3). The flights were conducted at an altitude ~100 m above the upper canopy and with a 70% overlap and 75% sidelap between adjacent images for front and side, respectively. Before each mission, the hyperspectral imager was calibrated using a white calibration panel to convert the digital number to reflectance value for collected images. Each flight mission data was processed using the Agisoft PhotoScan software (Agisoft, St. Petersburg, Russia) to generate mosaicked hyperspectral image covering the entire forest landscape, with an area of ~250 × 250 m^2 at a spatial resolution of ~0.16 m for each study site.

We processed the hyperspectral imagery as follows: First, we generated a Normalized Difference Vegetation Index (NDVI) mask using two bands of 672 and 864 nm, and then used a NDVI threshold of 0.7 to filter all the non-vegetation pixels, following Martin et al. (2018). Second, we generated the shadow mask using a site specific supervised maximum likelihood classifier (Richards, 2013) in ENVI (version 5.3, Exelis Visual Information Solutions, Boulder, CO, USA; Fig. S4), by which we filtered those shadow-contaminated pixels caused by gaps, self-shading or the adjacent taller canopies. Third, we followed Meacham-Hensold et al. (2020) and smoothed the canopy spectra on an image pixel basis using the Savitzky-Golay filter (Savitzky and Golay, 1964) for removing the high frequency noise with a second-order polynomial and a moving window of 15 spectral bands. Fourth, we performed brightness normalization on a pixel basis by dividing the entire spectral vector with its root sum of squares (Feilhauer et al., 2010). Notably, the brightness normalization method was used here because it reduced the impacts of sun angle and shadow on canopy spectra (Singh et al., 2015; Martin et al., 2018), reducing the variation of intra-crown spectra by ~56% (Fig. S5b and e) while increasing the ratio of the inter-crown to intra-crown spectral variation by ~35% (Fig. S5c and f).

During the same field campaigns, we also collected UAS-based LiDAR data with a LiAir V LiDAR system (GreenValley International, Berkeley, CA, USA) mounted on the same UAS as the hyperspectral imagery collected. With this LiDAR data, we derived leaf area index (LAI) using a 3-D voxelization method (Vincent et al., 2017). LAI is integrated from plant area density, which is dependent on the directional gap probability. The directional gap probability in the 3-D voxelization method is expressed as a function of the optical path length of a laser pulse through a voxel and the local extinction coefficient. For details regarding how we retrieved LAI from UAS-LiDAR refer to Method S2. Notably, the LiDAR-derived plant area index (PAI) includes both leaves and branches/woody materials, thus, in our retrieval of LAI, we followed Zou et al. (2009) and used a wood-total area ratio of 20% to account for the branch/woody material effect. Along with UAS-based hyperspectral and LiDAR measurements, we also conducted UAS surveys using a DJI Phantom 4 Advanced quadcopter (SZ DJI Technology Co., Ltd., Shenzhen, China) with a built-in 20MP RGB camera, to capture high-resolution RGB imagery and developed detailed RGB orthomosaics covering the entire forest landscape, with an area of ~250 × 250 m^2 at a spatial resolution of ~0.01 m. We cross-georeferenced the RGB, hyperspectral and LiDAR products of each site, and manually segmented the crown boundary polygons based on the georeferenced orthomosaic RGB images together with the in-situ field record of each canopy tree-crown/species. Finally, by integrating the tree-crown masks with pre-processed and quality-controlled hyperspectral imagery as described above, we further derived the crown-specific canopy spectra by extracting and averaging the canopy spectra of all the pixels within each crown boundary polygon. Some example demonstrations of the canopy spectra are provided in Fig. S6. Similarly, when integrating LiDAR-derived LAI with each individual tree-crown mask, we were able to derive the LAI metric for each individual tree crown.

2.3. Data analysis

2.3.1. Developing spectral models of foliar physiological, biochemical and morphological traits

In this study, we used partial least-squares regression (PLSR) (Wold et al., 2001) to infer foliar traits from leaf or canopy spectra within and across forest sites using the Python library 'scikit-learn' (Pedregosa et al., 2011). The PLSR method utilizes a dimensionality reduction transformation like principal component analysis (PCA) but takes the covariance between the response variable and the predictor variables into account, while having the advantage of direct interpretation of linear regression. Given this, PLSR is widely adopted in chemometric and spectroscopic analyses (Burnett et al., 2021).

Specifically, we followed the same approach as Dechant et al. (2017) and Yan et al. (2021) for our spectra-trait modelling, in which we integrated the PLSR analysis with the repeated double cross-validation (rdCV) method (Filzmoser et al., 2009). The rdCV first divided the whole dataset into calibration and independent validation subsets repeatedly with a cross-validation procedure, and then further divided the calibration subset into training and testing components with a second cross-validation procedure. This rdCV method can ensure that the actual model performance is evaluated on the independent validation subsets with many random splits and reduces the odds of randomly good or bad results. In our rdCV, we used 100 repeats, by which we generated an ensemble ($n = 100$) of PLSR models for each foliar trait. Detailed steps of rdCV are described in Method S3.

Foliar samples at two sites resulted in a total of 135 individual tree-crowns from 42 tree species, of which 124 had leaf gas exchange measurements (all samples had $V_{c,max25}$ but only 121 had enough data for curve fitting retrieval of J_{max25}). Notably, we assessed the potential uncertainty introduced by the mixed use of the two LiCOR types (LiCOR-6400 and 6800) and the results (Fig. S7) demonstrated that differences between instruments were minor at the species level. Therefore, we kept all the physiological measurements (regardless of LiCOR types) in the final analysis. Before spectral modelling, we followed Wang et al. (2020) and conducted rdCV PLSR to calculate the mean absolute error between measured and predicted values. We then identified and removed outliers for the 5% of data with the highest errors. As a result, we had 128 observations for LMA, LWC, Chl, N_{area} and P_{area}, 118 observations for $V_{c,max25}$ and 115 observations for J_{max25} (Table 1).

2.3.2. Exploring the canopy-level spectra-trait relationships under two modelling scenarios for the cross-site generalizability test

To explore whether the canopy-level spectra-trait relationships are generalizable across two sites, we performed the PLSR modelling under the following two scenarios. First, 'All-site' canopy spectral models of foliar traits were developed and evaluated using the PLSR analysis (same as Section 2.3.1) with all the data from the two forest sites. Second, 'Site-specific' canopy spectral models of foliar traits were developed and evaluated using the data from each of the two forest sites. The cross-comparisons of these two scenarios would help to understand whether a general spectral model could be developed and used for inferring each foliar trait from canopy spectra across the two sites.

Table 1
Summary of the data distribution for seven field-measured foliar traits at the tree-crown scale used in the spectral modelling of this study. These seven traits include leaf maximum carboxylation rate of RuBisCO standardized to 25 °C ($V_{c,max25}$), leaf maximum rate of electron transport standardized to 25 °C (J_{max25}), leaf mass per area (LMA), leaf water content (LWC), SPAD-based leaf chlorophyll content (Chl), area-based leaf nitrogen content (N_{area}), and area-based leaf phosphorus content (P_{area}). Six metrics were used to describe the data distribution of each foliar trait, including number of tree-crowns (n), minimum, maximum, mean, standard deviation (SD) and coefficient of variation (CV).

			Field measurements				
Trait	Unit	n	Min	Max	Mean	SD	CV
$V_{c,max25}$	μmol CO_2 m^{-2} s^{-1}	118	5.26	77.23	36.83	12.63	0.34
J_{max25}	μmol CO_2 m^{-2} s^{-1}	115	13.12	149.07	74.68	24.79	0.33
LMA	g m^{-2}	128	41.72	182.54	109.42	23.78	0.22
LWC	%	128	0.36	0.70	0.52	0.06	0.11
Chl	unitless	128	29.35	79.70	47.01	9.26	0.20
N_{area}	g m^{-2}	128	1.01	3.62	1.76	0.42	0.24
P_{area}	g m^{-2}	128	0.04	0.23	0.10	0.04	0.37

2.3.3. Assessing the canopy structure effect on spectra-trait relationships from leaf to canopy level

We had two sub-aims here: 1) to explore to what extent canopy structure impacts the spectra-trait relationships from the leaf to canopy scale, and if so, to what extent the impacts are similar or vary across the foliar traits, and 2) investigate whether the impacts of canopy structure on spectra-trait relationships can be captured by a commonly-used canopy radiative transfer model of 4SAIL (Verhoef et al., 2007). 4SAIL is based on the turbid medium assumption and is considered suitably applicable for mostly closed-canopy forest ecosystems like the two forest sites as examined in this study (le Maire et al., 2008). We used the PROSAIL model which is a combination of the PROSPECT leaf optical properties model (version PROSPECT-D; Féret et al., 2017) and the 4SAIL canopy bidirectional reflectance model to simulate canopy reflectance and approximate the influence of canopy structure on model performance. Here, we combined our field measurements of leaf reflectance with the PROSPECT model to simulate both leaf reflectance and transmittance spectra (Shiklomanov et al., 2016; Wu et al., 2018).

For sub-aim 1, the spectra-trait models developed with leaf spectra were directly transferred to the UAS-observed canopy spectra to evaluate the effect of canopy structure. The effect of canopy structure was smaller for traits if their leaf models display higher predictive accuracies when transferred to the canopy level, and vice versa. For sub-aim 2, we used PROSAIL to simulate canopy spectra, and then assessed the accuracy for foliar trait predictions when applying the spectra-trait models based on the simulated canopy spectra to the UAS-observed canopy spectra. High model accuracy indicates that PROSAIL captures critical canopy structural effects. The accuracy of model transferability was assessed using the correlation coefficient (r) between predicted vs. observed canopy foliar traits since there would have bias between leaf and canopy spectra, with the results from 'All-site' UAS-based canopy spectral models as the benchmark. We used the variable importance in projection (VIP) and spectral regression coefficients of PLSR to indicate the relative spectral contribution of each spectral model.

Specifically, three scenarios of spectra-trait models were trained and applied to the UAS-observed canopy spectra: 1) 'Leaf' model, in which field-measured leaf spectra and associated foliar traits were used to develop the spectra-trait models; 2) 'PROSAIL-fixed-LAI' model, in which we integrated field measurements of leaf spectra with PROSAIL to simulate canopy spectra with a fixed LAI scheme (assuming that all tree canopies from the same forest have the same LAI value), and then developed the canopy spectra-trait models based on the simulated canopy spectra and field-measured foliar traits; 3) 'PROSAIL-dynamic-LAI' model, which is overall similar as 'PROSAIL-fixed-LAI' model, and the only difference is using the tree-crown specific LAI. Notably, because we do not have the ground observation of LAI, besides LiDAR-derived LAI as Section 2.2.2 above, we retrieved another version of LAI directly from the UAS hyperspectral data using look-up-table (LUT) approach following Sinha et al. (2020); both versions of LAI are presented in the current study, with comparable modelling results and illustrated with details in later sections.

All these spectral models were trained using data from both sites, and the same PLSR modelling approach was used. To further minimize the effect associated with the use of different latent variables (i.e., a key parameter for PLSR modelling) across different modelling scenarios, for each foliar trait, we reported the results using the same number of latent

variables as the "All-site" canopy spectral model (Section 2.3.1) in the main text. Meanwhile, we also tested the modelling results using scenario-specific optimal latent variable for each foliar trait, and found that the model transferability would be even worse most likely due to the overfitting.

For all three modelling scenarios, we resampled the field-measured leaf spectra and PROSAIL-simulated canopy spectra (1 nm resolution, 400-2500 nm) into the same spectral resolution and the same spectral range as UAS canopy spectra (4 nm resolution, 93 bands, 502-870 nm). We used a Gaussian resampling approach with the sensor provided FWHM. Further, the leaf spectra or PROSAIL-simulated canopy spectra were brightness-normalized following the same method as used for UAS canopy spectra.

The parameterization used in PROSAIL is described in Table 2. More details about PROSAIL and associated two modelling scenarios of 'PROSAIL-fixed-LAI' and 'PROSAIL-dynamic-LAI' are shown in Method S4.

2.3.4. Mapping foliar traits using UAS-based imaging spectroscopy

To visualize and qualitatively analyze the trait variability across intra- and inter-specific levels, we mapped foliar traits at the tree-crown scale, including four steps. First, we used the ensemble 'All-site' UAS canopy spectral models (n = 100) to derive the per-pixel ensemble predictions. After these ensemble predictions, we then calculated the mean and standard deviation of predictions on a pixel and trait basis and repeated the procedure until all image pixels and all traits were calculated, by which we derived the maps of each foliar trait. Second, with the above trait maps, we followed Verrelst et al. (2016) to derive the prediction uncertainty (measured by coefficient of variation) on an image pixel and trait basis, and only kept those pixels with prediction uncertainty <25%. In addition, we also followed Wang et al. (2020) to filter those pixels with the predicted foliar trait value outside ±25% of the range of field-measured value, which were considered as unrealistic predictions. Third, we overlaid the retained image pixels with the manually created tree-crown masks (Section 2.2.2) and calculated the medians of the predicted trait values for all the retained pixels within each tree crown boundary to indicate foliar traits of each individual tree crown. Fourth, to visualize tree-crowns in a three-dimensional trait space, we created a R-G-B composite image using the rescaled, predicted tree-crown-scale trait values of LMA (for red band), $V_{c,max25}$ (for green band) and N_{area} (for blue band), with each band having the range of 0–1, corresponding to their respective trait values of minimum and maximum. These three foliar traits represent the morphological, physiological and biochemical dimension of functional traits, and are loosely correlated with each other (Fig. S9).

We further analyzed foliar trait variation within the UAS maps and compared the results with direct field measurements. We followed the method proposed by Guillén-Escribà et al. (2021) and adopted an analysis of variance (ANOVA)-based general linear modelling, by which we divided the field-/UAS-derived trait variability into interspecific and intraspecific components. Specifically, we fitted the species term and used the percentage sum of square explained by the species term to partition the total variance among individual tree-crowns into interspecific (species term) and intraspecific components (residual). The residual intraspecific variance could be attributed to many biotic and abiotic factors, such as ontogeny, genetic variation, and micro-environments. For this, we used the 'anova_lm' function in python package 'statsmodels' version 0.13 (Seabold and Perktold, 2010).

Table 2
Parameters and associated descriptions used in the Scattering by Arbitrarily Inclined Leaves (SAIL) model.

Parameter	Unit	PROSAIL-fixed-LAI	PROSAIL-dynamic-LAI
Varied parameters			
Leaf area index	$m^2\ m^{-2}$	Site-specific LiDAR-LAI or hyperspectra-LAI[1]	LiDAR-LAI or hyperspectra-LAI[2]
Leaf angle distribution	unitless	Six types[3]	Six types[3]
Fixed parameters			
Leaf reflectance	unitless	Inversed leaf reflectance[4]	Inversed leaf reflectance[4]
Leaf transmittance	unitless	Inversed leaf transmittance[5]	Inversed leaf transmittance[5]
Solar zenith angle[6]	°	10 for DH and 15 for XSBN	10 for DH and 15 for XSBN
Observer zenith angle	°	0	0
Relative azimuth angle	°	0	0
Hot spot factor[7]	unitless	0.004 ± 0.003	0.004 ± 0.003
Soil factor	unitless	0.25	0.25
Diffuse radiation fraction	unitless	From Eq.[8]	From Eq.[8]

[1] denotes the leaf area index (LAI) that was set up as the mean value of LiDAR-derived LAI or hyperspectra-derived LAI for each site. [2] denotes the LAI that was set up using the LAI value specific to each individual tree-crown based on either LiDAR-derived or hyperspectra-derived LAI. [3] denotes that the SAIL model was run for each of the six types of leaf angle distributions: Planophile, Erectophile, Plagiophile, Extremophile, Spherical, and Uniform. [4] denotes the directional-hemispherical leaf reflectance inversed from PROCOSINE model using field-measured reflectance spectra as input. PROCOSINE combines close-range spectral imaging of leaves model (COSINE) (Jay et al., 2016) with PROSPECT model. [5] denotes the PROCOSINE-inversed directional-hemispherical leaf transmittance using field-measured reflectance spectra as input. [6] the solar zenith angle was set up as that at the UAS flight time. [7] the hot spot factor was set for each individual crown and was estimated as the ratio of leaf width to tree height, which resulted in a range of 0.004 ± 0.003 (mean ± std). [8] the equation for calculating the diffuse radiation fraction (SKYL): $SKYL = 0.847 - 1.61 \times cos\,\theta_s + 1.04 \times cos^2\theta_s$, where θ_s indicates the solar zenith angle.

3. Results

3.1. Tree-crown scale foliar physiological traits from UAS-based imaging spectroscopy

We developed spectral models to infer the leaf physiological, morphological and biochemical traits (Table 1) from UAS-based imaging spectroscopy. We found that a single canopy spectral model covering all tree-crowns across the two forest sites (i.e., 'All-site' model) was able to capture the variation in key photosynthetic traits ($V_{c,max25}$; R^2 = 0.55, RMSE = 8.48 μmol CO_2 m^{-2} s^{-1}, nRMSE = 11.79%; J_{max25}, R^2 = 0.54, RMSE = 16.78 μmol CO_2 m^{-2} s^{-1}, nRMSE = 12.34%; Fig. 2 and Table S2). Similarly, the five other foliar traits were characterized with good accuracy (Fig. 2c-2g; Table S2), with LMA (R^2 = 0.50, RMSE = 16.78 g m^{-2}, nRMSE = 11.84%), LWC (R^2 = 0.38, RMSE = 0.05%, nRMSE = 13.48%), Chl (R^2 = 0.57, RMSE = 6.03, nRMSE = 11.97%), N_{area} (R^2 = 0.60, RMSE = 0.26 g m^{-2}, nRMSE = 10.11%), and P_{area} (R^2 = 0.59, RMSE = 0.02 g m^{-2}, nRMSE = 13.56%), showing robust model estimates.

Next, we investigated how the predictive accuracy of the canopy-scale 'Site-specific' models compared to the to the 'All-site' models. We found that the 'Site-specific' models of foliar physiological traits had slightly lower predictive accuracy than the 'All-site' models when pooling all the two sites' data together (R^2 = 0.49 vs 0.55 for $V_{c,max25}$; R^2 = 0.40 vs 0.54 for J_{max25}; Fig. 3a and b; Table S2). We e also found that compared to the 'Site-specific' models, the 'All-site' models yielded much lower prediction uncertainties as indicated by the smaller horizontal error bars (Fig. S10 vs. Fig. S11). Furthermore, we found the similar contrasts (in terms of the accuracy difference and prediction uncertainties) for the other five foliar morphological and biochemical traits (Figs. 3c-g, S10 and S11; Table S2).

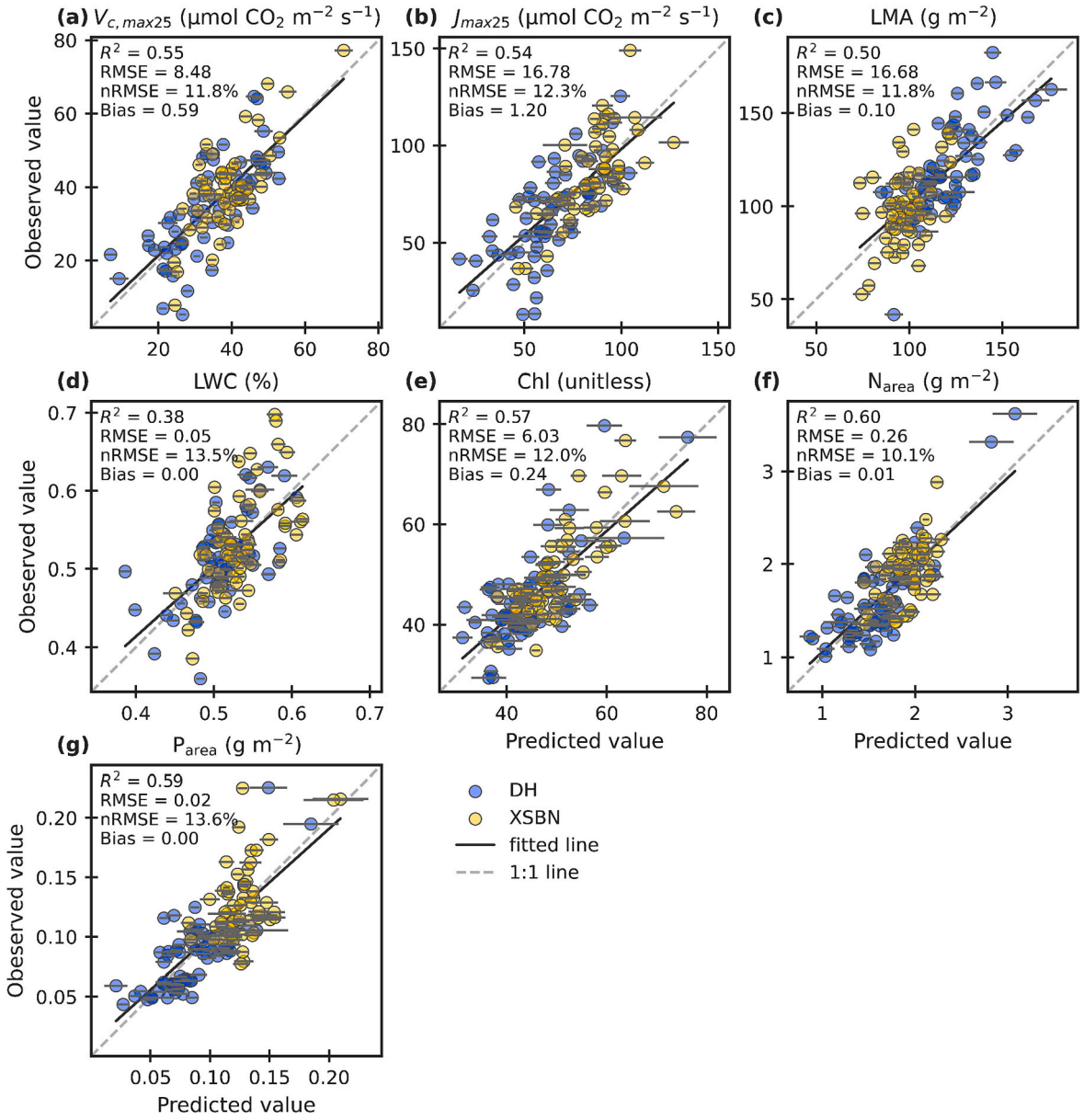

Fig. 2. Accuracy assessments for the 'All-site' canopy spectral models of foliar physiological, morphological, and biochemical traits, including (a) maximum carboxylation rate of RuBisCO standardized to 25 °C ($V_{c,max25}$), (b) maximum rate of electron transport standardized to 25 °C (J_{max25}), (c) leaf mass per area (LMA), (d) leaf water content (LWC), (e) SPAD-based leaf chlorophyll content (Chl), (f) area-based leaf nitrogen content (N_{area}), and (g) area-based leaf phosphorus content (P_{area}). The 'All-site' canopy spectral models were trained and evaluated using the data from all the two forest sites through the repeated double cross-validation method. Error bars indicate ±1 standard deviation for each predicted value derived from the ensemble partial least-squares regression (PLSR) models. The grey dashed line represents the 1:1 line, and the black line shows the fitted line of ordinary least-squares regression for all samples from the two forest sites. Two different colored circles indicate each of the two forest sites, with Mountain Dinghu (DH) in blue and Xishuangbanna (XSBN) in yellow. Abbreviations: R^2, the coefficient of determination; RMSE, root mean square error; nRMSE, normalized root mean square error; Bias, the residual bias. (For interpretation of the references to colour in this figure legend, the reader is referred to the web version of this article.)

3.2. *Transferability of spectra-trait relationships from leaf to canopy level*

We found evidence of poor transferability of 'Leaf' models to the canopy scale compared with the 'All-site' model based on UAS spectra (Figs. 4 and S13; Table S3). The closest agreement was found for LMA (r = 0.50 for 'Leaf' model vs r = 0.71 for UAS canopy model), followed by Chl (r = 0.45 vs 0.76), P_{area} (r = 0.39 vs 0.76) and $V_{c,max25}$ (r = 0.37 vs 0.74) with moderate agreement, and N_{area} (r = 0.19 vs 0.77), J_{max25} (r = 0.08 vs 0.73) and LWC (r = 0.07 vs 0.62) with low agreement. Moreover, the actual fits shown in Fig. S13 departed significantly from the 1:1 line, further demonstrating the far worse fits than the r values reported.

We also found that the 'PROSAIL-fixed-LAI' and 'PROSAIL-dynamic-LAI' models achieved very comparable results and generated overall similar patterns as the 'Leaf' models (Figs. 4, S14 and S15; Table S3), with much higher agreement in LMA (r = 0.57 for 'PROSAIL-fixed-LAI' model vs r = 0.71 for UAS canopy model) and N_{area} (r = 0.54 vs 0.77), followed by the moderate agreements in P_{area} (r = 0.51 vs 0.76), Chl (r = 0.50 vs 0.76), $V_{c,max25}$ (r = 0.41 vs 0.74) and J_{max25} (r = 0.26 vs 0.73), and the low agreement in LWC (r = 0.11 vs 0.62). We also observed slight improvements in model agreement for the 'PROSAIL-fixed-LAI' and 'PROSAIL-dynamic-LAI' models relative to the 'Leaf' models, with the absolute r increase ranging from 0.04 in LWC to 0.35 in N_{area}. Nevertheless, the actual fits shown in Fig. S14 and S15 again departed significantly from the 1:1 line, implying the low model transferability

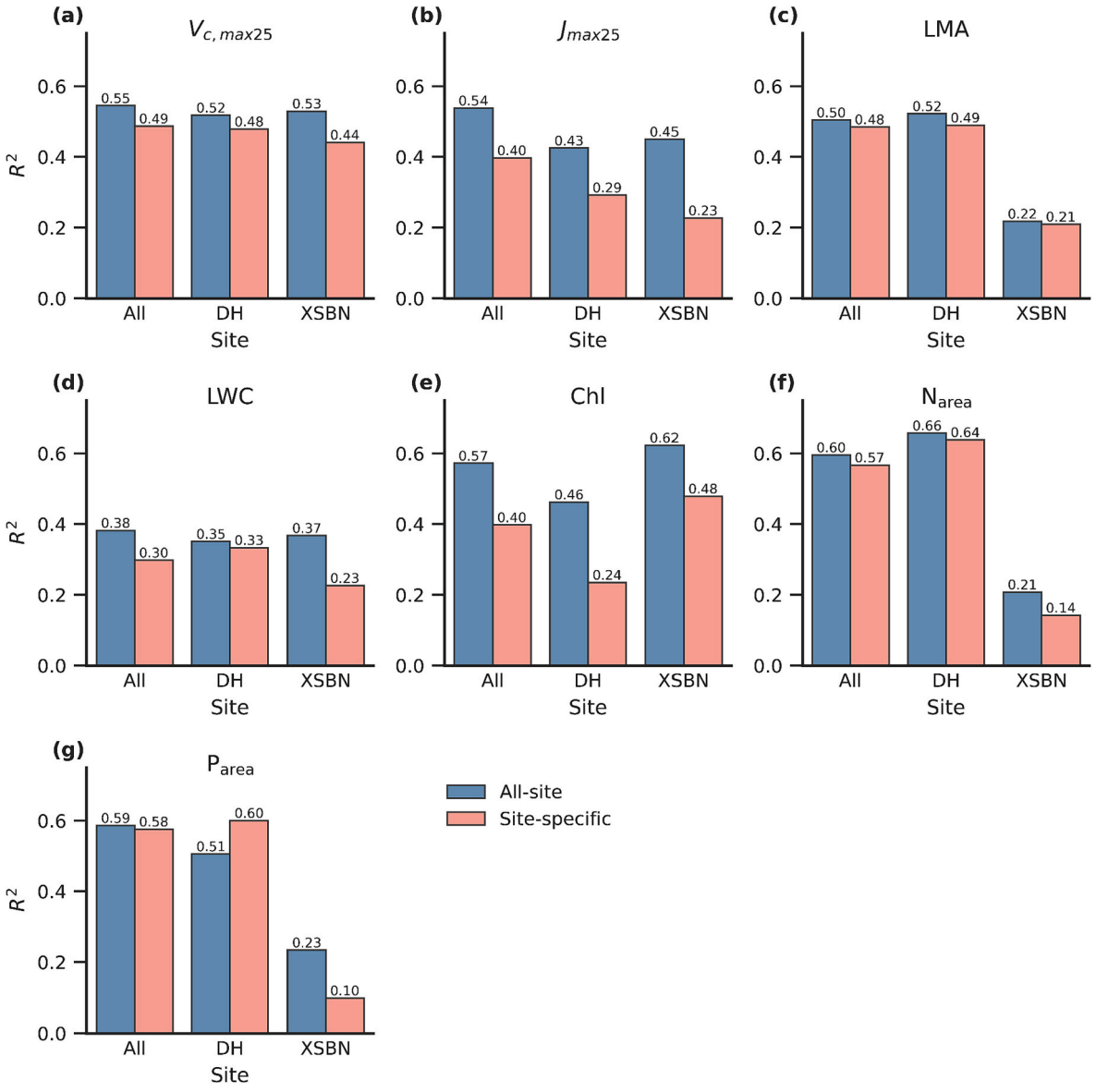

Fig. 3. Cross-comparison of the canopy spectral model performances of foliar physiological, morphological, and biochemical traits under the 'All-site' and 'Site-specific' scenarios. The 'All-site' spectral models (in blue) were trained and evaluated using the data from all the two forest sites through the repeated double cross-validation (rdCV) method. The 'Site-specific' models (in red) were trained and evaluated using the data from each forest site through the rdCV method. Bars indicate the values of coefficient of determination (R^2); Scatter plots for these spectral models under the two scenarios are provided inS10 and S11. (For interpretation of the references to colour in this figure legend, the reader is referred to the web version of this article.)

when using the PROSAIL process modelling approach.

We explored the potential drivers of the mismatch of leaf-to-canopy spectral model transferability by analyzing the model specific sensitive spectral regions for trait predictions (Fig. 5). Using $V_{c,max25}$ as an example, the VIP figure of the 'All-site' UAS-based canopy spectral model identified several important spectral domains for $V_{c,max25}$, including significant and dominant contribution (indicated by VIP > 1.0) from 690 to 766 nm, 774–786 nm, and 854–870 nm. For the 'Leaf' model, the VIP figure identified significant but dominant contribution from 502 to 510 nm, 638–734 nm, and 854–870 nm. While for the 'PROSAIL-fixed-LAI' and 'PROSAIL-dynamic-LAI' models, the VIP figures were nearly identical, with both identifying significant but dominant contribution from 522 to 560 nm, 678–754 nm, and 862–870 nm. In other words, certain sensitive spectral regions (e.g., 690–734 nm and 862–870 nm) are shared by all modelling scenarios, but each scenario also has specific sensitive spectral regions. Similarly, similarities and differences in the sensitive spectral regions across modelling scenarios were also observed for J_{max25} and the other five foliar traits (Fig. 5).

3.3. Mapping foliar traits using UAS-based imaging spectroscopy

Our results showed that UAS-imaging-derived foliar traits display large inter-crown variability, consistently at both sites (Figs. 6 and 7). $V_{c,max25}$ varied from 10 to 57 μmol CO_2 m^{-2} s^{-1} and J_{max25} varied from 26 to 103 μmol CO_2 m^{-2} s^{-1} at DH, and $V_{c,max25}$ varied from 13 to 60 μmol CO_2 m^{-2} s^{-1} and J_{max25} varied from 38 to 112 μmol CO_2 m^{-2} s^{-1} at XSBN. When overlapping these physiological trait maps with manually created tree-crown masks (Figs. 6j, 7j), we found that there were two primary sources of variation responsible for these observed inter-crown trait patterns (Table S4). At DH, at the intraspecies level, for example, *Castanea henryi* has a range of 20–57 μmol CO_2 m^{-2} s^{-1} in $V_{c,max25}$, and of 50–103 μmol CO_2 m^{-2} s^{-1} in J_{max25}; and *Schima superba* has a range of 13–44 μmol CO_2 m^{-2} s^{-1} in $V_{c,max25}$, and of 38–92 μmol CO_2 m^{-2} s^{-1} in J_{max25}; at the interspecies level, *Cinnamomum camphora* has the largest

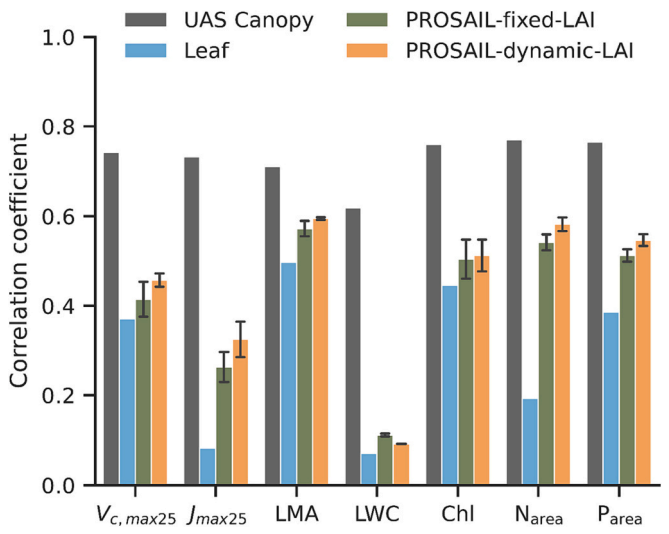

Fig. 4. Transferability of three spectral models to the UAS-observed canopy reflectance spectra for predicting foliar physiological, morphological, and biochemical traits, including the 'Leaf' spectral models, the 'PROSAIL-fixed-LAI' spectral models and the 'PROSAIL-dynamic-LAI' spectral models. The same UAS-based canopy spectral models as those in Fig. 2 are placed as the benchmark. The three models (i.e., 'Leaf', 'PROSAIL-fixed-LAI' and 'PROSAIL-dynamic-LAI' spectral models) were built based on field-measured leaf-scale reflectance spectra or PROSAIL simulated canopy reflectance spectra, and then applied to the UAS-observed canopy reflectance spectra for trait predictions. The mean of two ways of LAI parameterization (LiDAR-LAI or hyperspectra-LAI) for PROSAIL were displayed. Error bars indicate the range of PROSAIL modelling results respectively relying on LiDAR-LAI and hyperspectra-LAI as the model input. The PROSAIL model result with the 'Spherical' leaf angle distribution was displayed here; the PROSAIL model results with other leaf angle distributions were displayed in Fig. S16. Bars indicate the values of Pearson's correlation coefficients for the relationships between observed and predicted trait values.

species-level mean $V_{c,max25}$ of 41 μmol CO_2 m^{-2} s^{-1} and J_{max25} of 70 μmol CO_2 m^{-2} s^{-1}, and *Caryota ochlandra* has the lowest species-level mean $V_{c,max25}$ of 15 μmol CO_2 m^{-2} s^{-1} and J_{max25} of 39 μmol CO_2 m^{-2} s^{-1}. Similar inter-crown variations at the intraspecific and interspecific levels were also observed at XSBN (Table S4). Similar large crown-to-crown trait variability across both intraspecific and interspecific levels were observed for the other five morphological and biochemical traits (Fig. 6d-h in DH and Fig. 7d-h in XSBN).

We also visually analyzed the crown-to-crown variability from the multi-traits' perspective, using the three-trait-composite maps of DH and XSBN (Figs. 6i, 7i), with LMA for red band, $V_{c,max25}$ for green band, and N_{area} for blue band. We found that there was overall very high correspondence between the species map and the composite image for each of the two sites, with the tree-crowns of the same species tending to have similar R-G-B colour space in the composite trait map. These observations again demonstrate that species identity importantly affects the crown-scale trait variations. In addition, within each species, we also observed low-to-moderate R-G-B colour variations in the composite trait map, demonstrating that intraspecific variation is another source of factors influencing inter-crown trait variations.

An additional analysis was also performed to quantitatively partition the field-observed crown-scale trait variability into interspecific and intraspecific components. Our results show that the interspecific component dominates the explanations (Fig. 8; Tables S5 and S6). Specifically, at DH, P_{area} is best explained by interspecific variation (91.9%), followed by Chl (85.5%), N_{area} (84.1%), LWC (77.1%), LMA (76.7%), J_{max25} (53.6%) and $V_{c,max25}$ (53.0%); at XSBN, LWC is best explained by interspecific variation (89.5%), followed by Chl (87%), $V_{c,max25}$ (82.5%), J_{max25} (76.6%), LMA (65.3%), P_{area} (60.2%) and N_{area} (55.0%). In addition, we also found that the source of the trait variability predicted from the UAS-based imaging spectroscopy very well resembled the patterns as revealed by the direct field measurements (Fig. 8; Tables S5 and S6).

4. Discussion

4.1. Inferring foliar physiological traits from UAS-based imaging spectroscopy

Our results demonstrated, for-the-first-time, that in natural forest tree canopies a UAS-based imaging spectroscopy approach can characterize the inherent variations in foliar physiological traits of $V_{c,max25}$ and J_{max25} of subtropical and tropical forests (Fig. 2). This finding complements previous studies from agricultural systems that used piloted airborne imaging spectroscopy (Serbin et al., 2015) and ground mobile system (Fu et al., 2020; Meacham-Hensold et al., 2020), that also showed the capability to infer crop canopy physiological traits remotely. Compared with those previous examples from agricultural ecosystems, our results show a lower model performance (R^2), but given the simpler canopy structure of agricultural systems and quite comparable nRMSE, this suggests the approach is robust. The lower R^2 of this study is likely due to more complex canopy structure and narrower ranges of foliar physiological traits in our natural forests than those in agricultural ecosystems (Fu et al., 2020; Kumagai et al., 2021; Meacham-Hensold et al., 2020; Silva-Perez et al., 2018). For example, $V_{c,max}$ in Meacham-Hensold et al. (2020) had a range of 13.4 μmol m^{-2} s^{-1} to 359.3 μmol m^{-2} s^{-1}, ~5 times larger than ours. Another reason could be that much narrower spectral range (502–870 nm) was used in our imaging system relative to the wider spectral range (414–2447 nm) used in Serbin et al. (2015) and that (400–900 nm) in Fu et al. (2020).

We also found that a single 'All-site' spectral model could be developed for each foliar trait, and these models outperformed the 'Site-specific' models (Fig. 3 and Table S2). Although it is usually expected that 'Site-specific' spectral models will produce better or at least comparable results to 'All-site' spectral models (e.g., Yan et al., 2021), our study did not find this to be the case. This is likely due to the limited sample size and trait range on each site ($n = 67$ tree crowns for DH; $n = 61$ tree crowns for XSBN). Therefore, it is not surprising to see that the 'Site-specific' spectral model generated higher model uncertainty as indicated by the larger horizontal error bars (Fig. S10 vs. Fig. S11) and predicted less accurately compared to the 'All-site' spectral model when more abundant samples were used for model training. Additionally, the wider trait range resulting from pooling data from both sites (e.g., $V_{c,max25}$ = 5.26–77.23 μmol CO_2 m^{-2} s^{-1} for two sites vs. $V_{c,max25}$ = 5.26–64.66 μmol CO_2 m^{-2} s^{-1} for DH and 7.81–77.23 μmol CO_2 m^{-2} s^{-1} for XSBN) could also be attributed to the much larger sample size, resulting in more stable and accurate spectral modelling (Asner et al., 2011; Wu et al., 2019).

Although the broader-scale generalizability between plant spectral properties and traits at the leaf level have been widely reported previously (e.g., Nakaji et al., 2019; Serbin et al., 2019; Wu et al., 2019; Yan et al., 2021), our work extends this to the canopy for foliar physiological traits. As with previous research, we also demonstrate the potential of using imaging spectroscopy as a general approach for cross-site characterizations of foliar morphological and biochemical traits (Chlus and Townsend, 2022; Martin et al., 2008; Wang et al., 2020). Our findings, combined with those of previous studies, highlight the effectiveness of imaging spectroscopy in characterizing multiple foliar (e.g., morphological, biochemical, and physiological) trait variability across different scales. To improve understanding and accelerate progress towards robust methods that can work across a wider range of space, time and biological variation, we encourage additional data collection, open sharing of both spectral and trait data, and collaboration among those groups aiming to develop and apply these techniques.

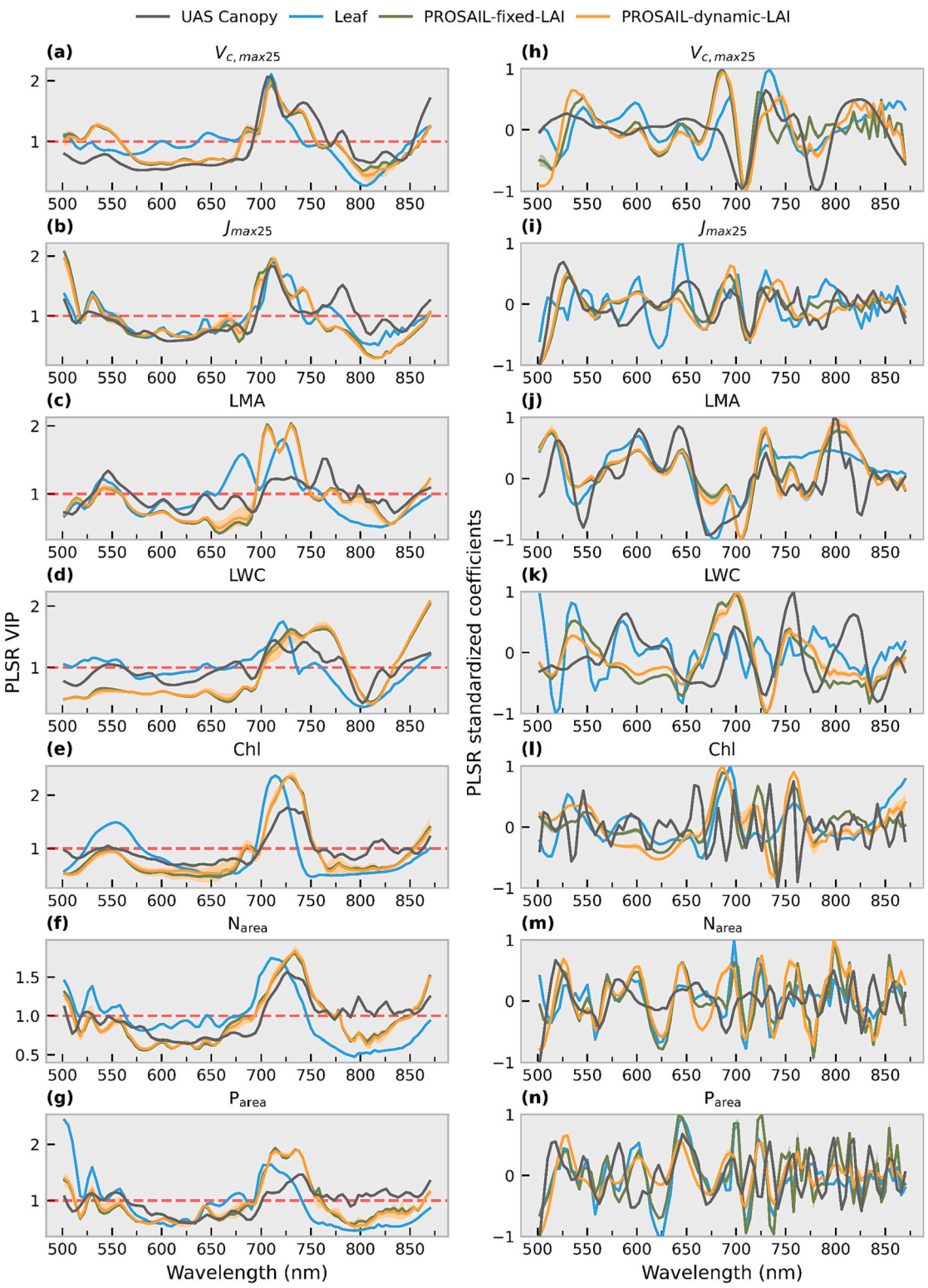

Fig. 5. Assessing the reflectance contributions to the spectral models of leaf physiological, morphological, and biochemical traits under the four scenarios using the partial least-squares regression (PLSR) approach, including the left panel (a-g) for the variable importance in projection (VIP), and the right panel (h-n) for PLSR regression coefficients. The four scenarios included the 'All-site' canopy spectral models as those in Fig. 2, the leaf spectral models, the 'PROSAIL-fixed-LAI' spectral models and the 'PROSAIL-dynamic-LAI' spectral models. The colored lines indicate the mean values of standardized PLSR regression coefficients and VIP spectrum, respectively. The mean of two ways of LAI parameterization (LiDAR-LAI or hyperspectra-LAI) were displayed for the 'PROSAIL-fixed-LAI' spectral models and the 'PROSAIL-dynamic-LAI' spectral models. Shaded regions indicate the range of results of using two ways for LAI parameterization. On the left panel, the red dashed line represents VIP of 1, which was suggested as the threshold to identify the sensitive spectral regions for the spectral modelling (Wold et al., 2001). All the PLSR coefficients were standardized to a range of −1 to 1. (For interpretation of the references to colour in this figure legend, the reader is referred to the web version of this article.)

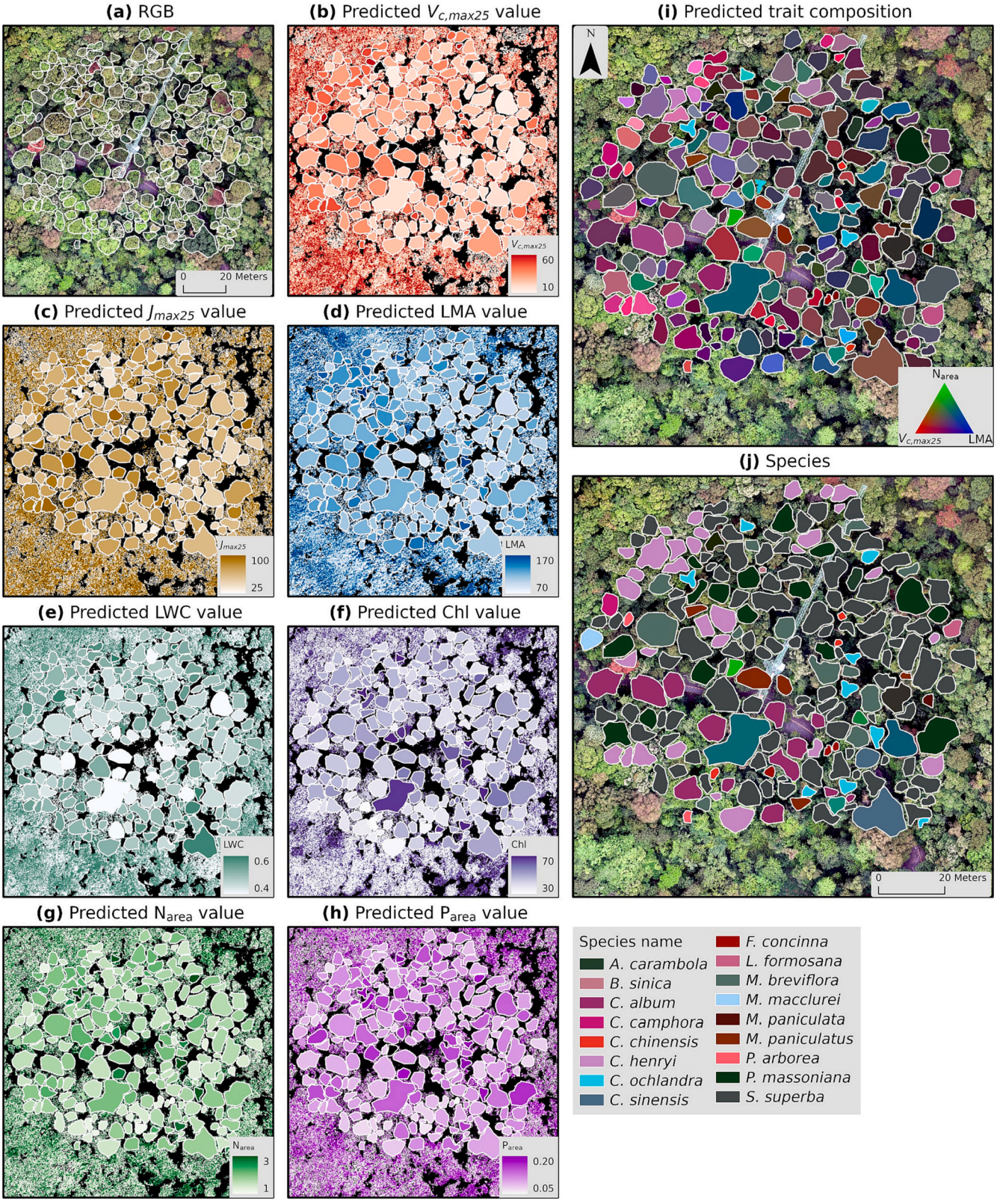

Fig. 6. Maps of canopy tree-crown RGB image based on a UAS survey at the Mt. Dinghu site (a), spatial variations in the seven traits (b-h), RGB composited image (i) of $V_{c,max25}$ (red), N_{area} (green) and LMA (blue), and field-identified tree species distribution (j). These trait maps were derived from the "All-site" canopy spectral models of foliar traits. Different geometric polygons indicate manually identified canopy tree-crowns, with white borders representing the crown boundaries. The UAS-based hyperspectral image is used to derive the pixel-level leaf traits, and then the medians of the predicted trait values for all pixels within each tree crown boundary were displayed here. In panels (b-h), the black areas indicate pixels that are filtered with low NDVI values, shadows or high uncertainty in the trait prediction. In panel (j), the colors represent different tree species, with a total of 17 canopy tree species. (For interpretation of the references to colour in this figure legend, the reader is referred to the web version of this article.)

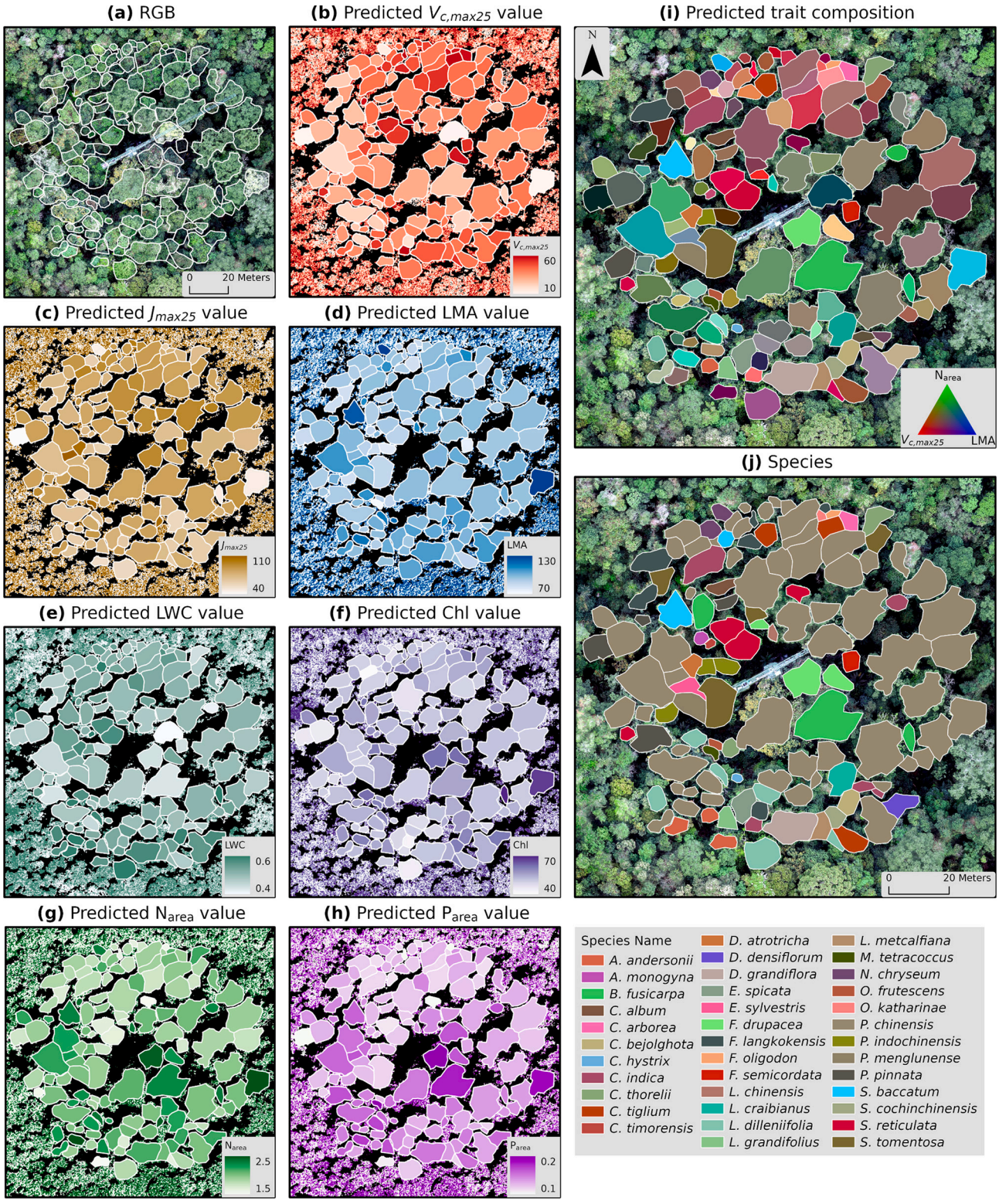

Fig. 7. Maps of canopy tree-crown RGB image based on a UAS survey at the Xishuangbanna site (a), spatial variations in the seven traits (b-h), RGB composited image (i) of $V_{c,max25}$ (red), N_{area} (green) and LMA (blue), and field-identified tree species distribution (j). These trait maps were derived from the "All-site" canopy spectral models of foliar traits. Different geometric polygons indicate manually identified canopy tree-crowns, with white borders representing the crown boundaries. The UAS-based hyperspectral image is used to derive the pixel-level leaf traits, and then the medians of the predicted trait values for all pixels within each tree crown boundary were display here. In panels (b-h), the black areas indicate pixels that are filtered with low NDVI values, shadows or high uncertainty in the trait prediction. In panel (j), the colors represent different tree species, with a total of 37 canopy tree species. (For interpretation of the references to colour in this figure legend, the reader is referred to the web version of this article.)

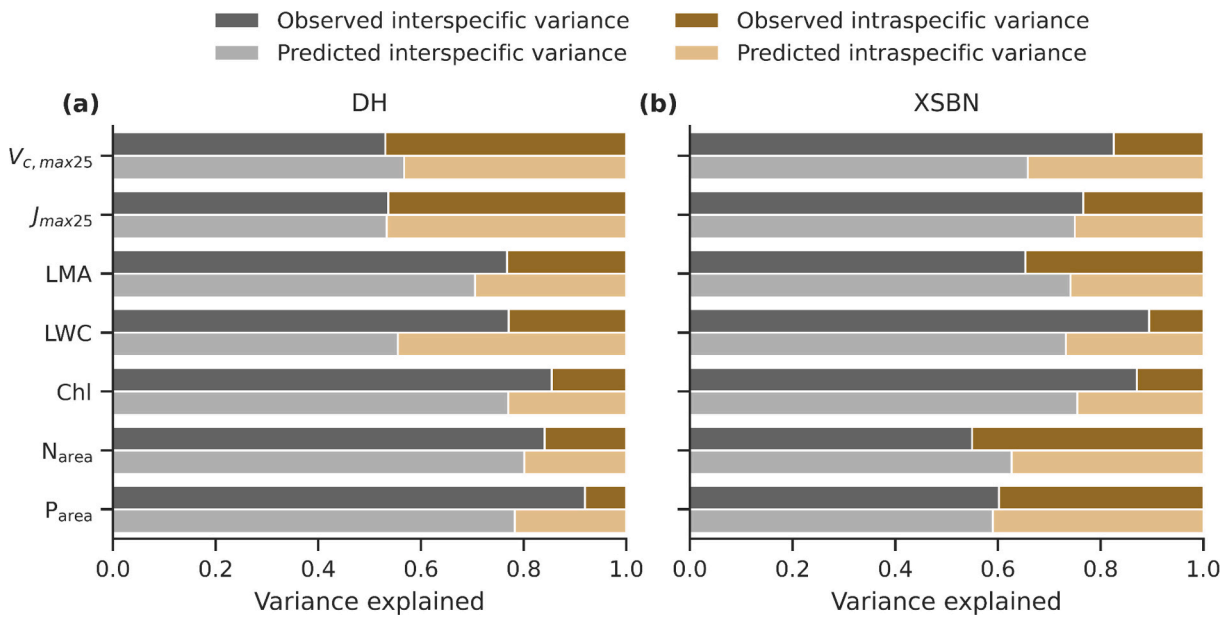

Fig. 8. Variance partitioning of foliar physiological, morphological, and biochemical traits at DH and XSBN sites. The total variability for each trait was partitioned into the interspecific and intraspecific components. The darker colour indicates the variance partitioning results from field-observed foliar traits, while lighter colour indicates the variance partitioning results from foliar traits predicted from UAS-based imaging spectroscopy.

4.2. The effect of canopy structure on the spectra-trait relationships from leaf to canopy level

Leaf optical properties have long been hypothesized as a key basis of canopy imaging spectroscopy (Baret et al., 1994). Our results demonstrate that the transferability of spectra-trait relationships from leaf to canopy level varies considerably across foliar traits, with modest cross-level transferability in LMA and Chl, and low transferability in the physiological (i.e., $V_{c,max25}$ and J_{max25}) and other biochemical traits (i.e., LWC, N_{area} and P_{area}) (Fig. 4). The underlying reason is largely because absorption processes dominate canopy reflectance in the visible part of the spectrum, while scattering processes dominate the NIR spectrum (Fig. S17; Asner, 1998; Kokaly et al., 2009; Ustin et al., 2009; Wu et al., 2019). Since the two processes depend on both leaf optical properties and canopy structure, high visible light absorption means that the light only shows minor scattering and the leaf and canopy level reflectance differ primarily due to differences in shadowing. While in the NIR, the low absorptance and high transmittance of leaves propagate to canopy reflectance spectra though canopy structure, resulting in high scattering (Roberts et al., 2004).

Because of these distinct contributions of leaf spectra and canopy structure to canopy spectra, it is thus not surprising to see the relatively higher cross-level spectral model transferability in LMA and Chl (Fig. 4), as these traits show higher dependence on the visible reflectance spectra (dominated by leaf spectra). Other traits (e.g., $V_{c,max25}$, J_{max25}, LWC, and N_{area}) exhibit higher dependence on canopy NIR reflectance (Fig. 5), where leaf spectra have little contribution, thus resulting in the much lower cross-level transferability of these traits (Fig. 4). Interestingly, we found that 'Leaf' models had low model transferability for characterizing canopy foliar N_{area} ($r = 0.19$ vs 0.77), but the 'PROSAIL-dynamic-LAI' models showed large improvement ($r = 0.57$ vs 0.77), likely because canopy structure dominates the canopy spectral model of foliar N_{area} as hypothesized by Knyazikhin et al. (2013).

Since canopy structure is important in affecting the transferability of spectra-trait relationships from leaf to canopy level, we next investigated whether the commonly used 4SAIL model could capture such canopy structural effects. Our results indicate that although PROSAIL can capture canopy structural effects to some extent for certain foliar traits, such as LMA and Chl, it may not consistently capture these effects for other traits, regardless of the LAI version used (e.g., LiDAR- vs. hyperspectra-derived LAI) (Fig. 4). The underlying reason could be largely associated with the canopy structural diversity among tree individuals in our studied sites (Yi et al., 2022), which includes the diversity covering multi-dimensional canopy structure attributes (e.g., LAI, surface rugosity, leaf angle distribution, vertical profile of leaf area, etc.). As a result, the simple canopy radiative transfer model of 4SAIL could not well capture such complex canopy structural effects, especially those structural variables beyond LAI. This interpretation is supported by studies that integrated terrestrial LiDAR-derived 3-D canopy structure with more sophisticated canopy radiative transfer models (e.g., FLiES (Kobayashi et al., 2012), DART (Gastellu-Etchegorry et al., 2015) or others) and found large simulated canopy reflectance differences when compared with the 4SAIL results (Ferreira et al., 2018; Timmermans et al., 2008; Wu et al., 2018). In other words, although 4SAIL might be efficient in capturing the LAI effect on canopy reflectance spectra (Fig. 4), other dimensions of canopy structural attributes (e.g., leaf angle distribution, etc.) might be more important regulators of the spectra-trait relationships in the real-world forest tree canopies, but not yet effectively captured by the 4SAIL model. Therefore, it should be cautioned that the canopy reflectance is not just simply adding canopy structural signals (like LAI) with a few leaf reflectance measurements.

Our results also generate at least two implications. First, the integration of the PROSPECT model with leaf spectra and other representations of canopy structure (e.g., LiDAR, ecosystem demography models, or others) has been suggested as a way to explore practical and broad-scale applicability of canopy spectra-trait models, by which various canopy level spectral measurements (from UAS, airplane, and satellites) can be assimilated for foliar trait predictions (Abdelbaki et al., 2021; Shiklomanov et al., 2021; Tagliabue et al., 2022; Verrelst et al., 2021). However, our work raises concern regarding this approach, as the complexity of the canopy structural effects would make the spectra-trait relationships less transferable from the leaf to canopy level, and difficult to be captured by process-based radiative transfer models. Second, since canopy structure importantly regulates canopy spectra-trait relationships but is difficult to be captured by 4SAIL, our results further suggest that the broader-scale field campaigns of both canopy spectra and foliar physiological traits would be one of the most important alternatives for directly exploring the large-scale applicable imaging spectroscopy

approach for foliar physiological trait characterizations.

4.3. Foliar trait mapping and implications underlying the inter-crown trait variability

Our research provides at least two implications for plant functional ecology research. First, our study demonstrates that UAS-based imaging spectroscopy can improve the monitoring efficiency and spatial extent of foliar trait characterizations, especially when comparing with conventional field-based monitoring methods. As illustrated in this study, the UAS imaging spectroscopy enables tree-crown-scale monitoring of foliar traits, maps foliar traits covering the forest landscapes with spatially explicit information, and offers a high-throughput means to characterizing multi-dimensional foliar traits ranging from morphological, biochemical to physiological traits (Figs. 6 and 7). Meanwhile, combined with the individual tree-crown boundaries obtained from the field investigation (or high-resolution aerial photograph), the UAS-based imaging spectroscopy also allows accurate mapping of traits at the individual tree-crown level with relevant species information. Individual trees are the basic unit for scaling plant functional traits from the organism to the ecosystem level (Violle et al., 2007), but it is challenging to do this from field plot-based or remote sensing image-pixel-based studies (Asner et al., 2015; Meacham-Hensold et al., 2020; Wang et al., 2020) where the contribution of individual trees is lost. Our proposed individual tree-crown level trait mapping offers a unique opportunity to examine the trait variability across intra- and inter-specific levels (Figs. 6, 7, and 8; Tables S6 and S7), as well as to understand how the fine-scale trait variability ultimately determines the ecosystem level trait value and diversity.

Second, the imaging spectroscopy-derived tree-crown scale foliar traits contribute to an important dataset that could advance plant functional ecology studies. Relevant potential topics include but are not limited to interpreting the trait variability and trait-trait coordinated relationships across various ecological levels (e.g., from organisms to ecosystems), exploring the proximate (related with both micro- and macro- environmental conditions) and ultimate (related with fundamental eco-evolutionary principles) drivers of foliar trait variability, and assessing the roles of plant functional diversity in regulating many important ecosystem processes, functioning, and resilience/vulnerability response to climate change (Durán et al., 2019; Feilhauer et al., 2018; Schneider et al., 2017; Schweiger et al., 2018; Wang et al., 2022; Wieczynski et al., 2022; Zheng et al., 2021). Moreover, since $V_{c,max25}$ and J_{max25} are arguably two of the most important parameters for modelling plant photosynthesis, their availability would offer a potential to simulate and map plant photosynthesis at the tree-crown scale. Such data can also help explore how these fine-scale physiological trait variability would affect the simulations of ecosystem-level physiological and sensitivity responses to current and future climate change (Bernacchi et al., 2013; Jetz et al., 2016; Kattge et al., 2009; Rogers, 2014). The mapped plant photosynthetic capacity might be also useful to evaluate several satellite proxies of canopy photosynthesis, such as solar-induced fluorescence (SIF), near-infrared reflectance of vegetation (NIR_V) and near-infrared reflectance of vegetation multiplied by incoming sunlight (NIR_VP) (Zeng et al., 2022), and uncover the key biophysical mechanisms (related with physiological traits, canopy structure, and physiological response to various environmental stressors) underlying the spatiotemporal variability in these satellite photosynthetic proxies.

5. Conclusion

In this study, we used data from two forest sites in Southern China to demonstrate that UAS-based imaging spectroscopy can be an effective and cross-site generalizable method for characterizing tree-crown scale physiological ($V_{c,max25}$ and J_{max25}), morphological and biochemical traits (i.e., LMA, LWC, Chl, N_{area}, and P_{area}) (Figs. 2 and 3). We also found that canopy structure altered spectra-trait relationships from leaf to canopy level, and such effects varied considerably across foliar traits and were not adequately captured by the 4SAIL canopy radiative transfer model (Fig. 4). Thirdly, UAS-based imaging spectroscopy can map spatially explicit variations in all foliar traits (including physiological traits) shaped by both intra- and inter-specific components (Figs. 6, 7, and 8). These maps provide a critical dataset for assessing foliar trait variability across various levels, as well as understanding the theory underlying trait-trait coordination. These findings suggest that imaging spectroscopy has the capability to map foliar photosynthetic capacity at both fine and ecosystem scale, with potential to be extended to even larger spatial extents.

Author contribution statement

Jin Wu, Zhengbing Yan, and Shuwen Liu conceived the project idea, and designed the research. Zhengbing Yan, Shuwen Liu, Guangqin Song, Qianhan Wu, and Zhengfei Guo collected the field data with support from Jinlong Dong. Shuwen Liu and Zhengbing Yan performed the data analysis. Jin Wu, Zhengbing Yan, and Shuwen Liu interpreted the results, with significant input from Zhihui Wang, Shawn Serbin, Marco Visser, Yuan Zeng, Yongeryel Ryu, Yanjun Su, He Zhang, Billy Chi Hang Hau, Ping Zhao, Xi Yang, Lingli Liu, and Alistair Rogers. Shuwen Liu, Zhengbing Yan, and Jin Wu drafted the manuscript, and all authors contributed to the manuscript editing and revision.

Declaration of Competing Interest

The authors declare that they have no known competing financial interests or personal relationships that could have appeared to influence the work reported in this paper.

Data availability

Data will be made available on request.

Acknowledgements

We would like to thank the editors and three reviewers for providing valuable suggestions and comments, which are greatly helpful in improving the quality of this work. The work was primarily supported by National Natural Science Foundation of China (#31922090), Hong Kong Research Grant Council Early Career Scheme (#27306020) and General Research Fund (#17305321), and the Centre for Slope Safety (AoE/E-603/18) of the Research Grants Council of the Hong Kong SAR Government. YZ and JW were in part supported by the HKU Seed Funding for Basic Research (202011159154) and the HKU Seed Funding for Strategic Interdisciplinary Research Scheme and the Innovation. JW was in part supported by the Innovation and Technology Fund (funding support to State Key Laboratories in Hong Kong of Agrobiotechnology) of the HKSAR, China. ZW was supported by GDAS' Special Project of Science and Technology Development (2020GDASYL-20200102001). AR and SPS were supported by the Next-Generation Ecosystem Experiments -Tropics project that is supported by the Office of Biological and Environmental Research in the Department of Energy, Office of Science, and through the United States Department of Energy contract No. DE-SC0012704 to Brookhaven National Laboratory. SPS was additionally supported by the NASA Surface Biology and Geology Mission Study (80GSFC22TA016). YR was supported by Ministry of Environment of Korea (2022003640002). The authors thanks Dr. Md Mizanur Rahman for the discussion in the early stage of the manuscript. The authors would like to thank the National Forest Ecosystem Research Stations at Xishuangbanna, Wenfu Zhang for canopy crane access assistance.

Appendix A. Supplementary data

Supplementary data to this article can be found online at https://doi.org/10.1016/j.rse.2023.113612.

References

Abdelbaki, A., Schlerf, M., Retzlaff, R., Machwitz, M., Verrelst, J., Udelhoven, T., 2021. Comparison of crop trait retrieval strategies using UAV-based VNIR hyperspectral imaging. Remote Sens. 13, 1–25. https://doi.org/10.3390/rs13091748.

Albert, L.P., Wu, J., Prohaska, N., de Camargo, P.B., Huxman, T.E., Tribuzy, E.S., Ivanov, V.Y., Oliveira, R.S., Garcia, S., Smith, M.N., Oliveira Junior, R.C., Restrepo-Coupe, N., da Silva, R., Stark, S.C., Martins, G.A., Penha, D.V., Saleska, S.R., 2018. Age-dependent leaf physiology and consequences for crown-scale carbon uptake during the dry season in an Amazon evergreen forest. New Phytol. 219, 870–884. https://doi.org/10.1111/nph.15056.

Ali, A.A., Xu, C., Rogers, A., McDowell, N.G., Medlyn, B.E., Fisher, R.A., Wullschleger, S. D., Reich, P.B., Vrugt, J.A., Bauerle, W.L., Santiago, L.S., Wilson, C.J., 2015. Global-scale environmental control of plant photosynthetic capacity. Ecol. Appl. 25, 2349–2365. https://doi.org/10.1890/14-2111.1.

Asner, G.P., 1998. Biophysical and biochemical sources of variability in canopy reflectance. Remote Sens. Environ. 64, 234–253. https://doi.org/10.1016/S0034-4257(98)00014-5.

Asner, G.P., Martin, R.E., 2008. Spectral and chemical analysis of tropical forests: scaling from leaf to canopy levels. Remote Sens. Environ. 112, 3958–3970. https://doi.org/10.1016/j.rse.2008.07.003.

Asner, G.P., Martin, R.E., Anderson, C.B., Knapp, D.E., 2015. Quantifying forest canopy traits: imaging spectroscopy versus field survey. Remote Sens. Environ. 158, 15–27. https://doi.org/10.1016/j.rse.2014.11.011.

Asner, G.P., Martin, R.E., Knapp, D.E., Tupayachi, R., Anderson, C., Carranza, L., Martinez, P., Houcheime, M., Sinca, F., Weiss, P., 2011. Spectroscopy of canopy chemicals in humid tropical forests. Remote Sens. Environ. 115, 3587–3598. https://doi.org/10.1016/j.rse.2011.08.020.

Baret, F., Vanderbilt, V.C., Steven, M.D., Jacquemoud, S., 1994. Use of spectral analogy to evaluate canopy reflectance sensitivity to leaf optical properties. Remote Sens. Environ. 48, 253–260. https://doi.org/10.1016/0034-4257(94)90146-5.

Bernacchi, C.J., Bagley, J.E., Serbin, S.P., Ruiz-Vera, U.M., Rosenthal, D.M., Vanloocke, A., 2013. Modelling C3 photosynthesis from the chloroplast to the ecosystem. Plant Cell Environ. 36, 1641–1657. https://doi.org/10.1111/pce.12118.

Bernacchi, C.J., Pimentel, C., Long, S.P., 2003. In vivo temperature response functions of parameters required to model RuBP-limited photosynthesis. Plant Cell Environ. 26, 1419–1430. https://doi.org/10.1046/j.0016-8025.2003.01050.x.

Bonan, G.B., Doney, S.C., 2018. Climate, ecosystems, and planetary futures: the challenge to predict life in earth system models. Science 359. https://doi.org/10.1126/science.aam8328.

Burnett, A.C., Anderson, J., Davidson, K.J., Ely, K.S., Lamour, J., Li, Q., Morrison, B.D., Yang, D., Rogers, A., Serbin, S.P., 2021. A best-practice guide to predicting plant traits from leaf-level hyperspectral data using partial least squares regression. J. Exp. Bot. 72, 6175–6189. https://doi.org/10.1093/jxb/erab295.

Burnett, A.C., Davidson, K.J., Serbin, S.P., Rogers, A., 2019. The "one-point method" for estimating maximum carboxylation capacity of photosynthesis: a cautionary tale. Plant Cell Environ. 42, 2472–2481. https://doi.org/10.1111/pce.13574.

Cao, M., Zou, X., Warren, M., Zhu, H., 2006. Tropical forests of xishuangbanna, China1. Biotropica 38, 306–309. https://doi.org/10.1111/j.1744-7429.2006.00146.x.

Chavana-Bryant, C., Malhi, Y., Wu, J., Asner, G.P., Anastasiou, A., Enquist, B.J., Cosio Caravasi, E.G., Doughty, C.E., Saleska, S.R., Martin, R.E., Gerard, F.F., 2017. Leaf aging of amazonian canopy trees as revealed by spectral and physiochemical measurements. New Phytol. 214, 1049–1063. https://doi.org/10.1111/nph.13853.

Chen, L., Zhang, Y., Nunes, M.H., Stoddart, J., Khoury, S., Chan, A.H.Y., Coomes, D.A., 2022. Predicting leaf traits of temperate broadleaf deciduous trees from hyperspectral reflectance: can a general model be applied across a growing season? Remote Sens. Environ. 269, 112767 https://doi.org/10.1016/j.rse.2021.112767.

Chlus, A., Townsend, P.A., 2022. Characterizing seasonal variation in foliar biochemistry with airborne imaging spectroscopy. Remote Sens. Environ. 275, 113023 https://doi.org/10.1016/j.rse.2022.113023.

Coste, S., Baraloto, C., Leroy, C., Marcon, É., Renaud, A., Richardson, A.D., Roggy, J.-C., Schimann, H., Uddling, J., Hérault, B., 2010. Assessing foliar chlorophyll contents with the SPAD-502 chlorophyll meter: a calibration test with thirteen tree species of tropical rainforest in French Guiana. Ann. For. Sci. 67, 607.

Croft, H., Chen, J.M., Luo, X., Bartlett, P., Chen, B., Staebler, R.M., 2017. Leaf chlorophyll content as a proxy for leaf photosynthetic capacity. Glob. Change Biol. 23, 3513–3524. https://doi.org/10.1111/gcb.13599.

Curran, P.J., 1989. Remote sensing of foliar chemistry. Remote Sens. Environ. 30, 271–278. https://doi.org/10.1016/0034-4257(89)90069-2.

Dawson, T.P., Curran, P.J., North, P.R.J., Plummer, S.E., 1999. The propagation of foliar biochemical absorption features in Forest canopy reflectance: a theoretical analysis. Remote Sens. Environ. 67, 147–159. https://doi.org/10.1016/S0034-4257(98)00081-9.

De Kauwe, M.G., Lin, Y.S., Wright, I.J., Medlyn, B.E., Crous, K.Y., Ellsworth, D.S., Maire, V., Prentice, I.C., Atkin, O.K., Rogers, A., Niinemets, Ü., Serbin, S.P., Meir, P., Uddling, J., Togashi, H.F., Tarvainen, L., Weerasinghe, L.K., Evans, B.J., Ishida, F.Y., Domingues, T.F., 2016. A test of the "one-point method" for estimating maximum carboxylation capacity from field-measured, light-saturated photosynthesis. New Phytol. 210, 1130–1144. https://doi.org/10.1111/nph.13815.

Dechant, B., Cuntz, M., Vohland, M., Schulz, E., Doktor, D., 2017. Estimation of photosynthesis traits from leaf reflectance spectra: correlation to nitrogen content as the dominant mechanism. Remote Sens. Environ. 196, 279–292. https://doi.org/10.1016/j.rse.2017.05.019.

Doughty, C.E., Santos-Andrade, P.E., Goldsmith, G.R., Blonder, B., Shenkin, A., Bentley, L.P., Chavana-Bryant, C., Huaraca-Huasco, W., Díaz, S., Salinas, N., Enquist, B.J., Martin, R., Asner, G.P., Malhi, Y., 2017. Can leaf spectroscopy predict leaf and Forest traits along a peruvian tropical Forest elevation Gradient? J. Geophys. Res. Biogeosci. 122, 2952–2965. https://doi.org/10.1002/2017JG003883.

Durán, S.M., Martin, R.E., Díaz, S., Maitner, B.S., Malhi, Y., Salinas, N., Shenkin, A., Silman, M.R., Wieczynski, D.J., Asner, G.P., Bentley, L.P., Savage, V.M., Enquist, B. J., 2019. Informing trait-based ecology by assessing remotely sensed functional diversity across a broad tropical temperature gradient. Sci. Adv. 5, 1–12. https://doi.org/10.1126/sciadv.aaw8114.

Elvidge, C.D., 1990. Visible and near infrared reflectance characteristics of dry plant materials. Int. J. Remote Sens. 11, 1775–1795. https://doi.org/10.1080/01431169008955129.

Ely, K.S., Burnett, A.C., Lieberman-Cribbin, W., Serbin, S.P., Rogers, A., 2019. Spectroscopy can predict key leaf traits associated with source–sink balance and carbon–nitrogen status. J. Exp. Bot. 70, 1789–1799. https://doi.org/10.1093/jxb/erz061.

Farquhar, G.D., Caemmerer, S., Berry, J.A., 1980. A biochemical model of photosynthetic CO2 assimilation in leaves of C3 species. Planta 149, 78–90–90.

Feilhauer, H., Asner, G.P., Martin, R.E., Schmidtlein, S., 2010. Brightness-normalized partial least squares regression for hyperspectral data. J. Quant. Spectrosc. Radiat. Transf. 111, 1947–1957. https://doi.org/10.1016/j.jqsrt.2010.03.007.

Feilhauer, H., Schmid, T., Faude, U., Sánchez-Carrillo, S., Cirujano, S., 2018. Are remotely sensed traits suitable for ecological analysis? A case study of long-term drought effects on leaf mass per area of wetland vegetation. Ecol. Indic. 88, 232–240. https://doi.org/10.1016/j.ecolind.2018.01.012.

Féret, J.B., le Maire, G., Jay, S., Berveiller, D., Bendoula, R., Hmimina, G., Cheraiet, A., Oliveira, J.C., Ponzoni, F.J., Solanki, T., de Boissieu, F., Chave, J., Nouvellon, Y., Porcar-Castell, A., Proisy, C., Soudani, K., Gastellu-Etchegorry, J.P., Lefèvre-Fonollosa, M.J., 2019. Estimating leaf mass per area and equivalent water thickness based on leaf optical properties: potential and limitations of physical modeling and machine learning. Remote Sens. Environ. 231, 110959 https://doi.org/10.1016/j.rse.2018.11.002.

Ferreira, M.P., Féret, J.B., Grau, E., Gastellu-Etchegorry, J.P., Shimabukuro, Y.E., de Souza Filho, C.R., 2018. Retrieving structural and chemical properties of individual tree crowns in a highly diverse tropical forest with 3D radiative transfer modeling and imaging spectroscopy. Remote Sens. Environ. 211, 276–291. https://doi.org/10.1016/j.rse.2018.04.023.

Filzmoser, P., Liebmann, B., Varmuza, K., 2009. Repeated double cross validation. J. Chemom. 23, 160–171. https://doi.org/10.1002/cem.1225.

Fu, P., Meacham-Hensold, K., Guan, K., Wu, J., Bernacchi, C., 2020. Estimating photosynthetic traits from reflectance spectra: a synthesis of spectral indices, numerical inversion, and partial least square regression. Plant Cell Environ. 43, 1241–1258. https://doi.org/10.1111/pce.13718.

Gastellu-Etchegorry, J.P., Yin, T., Lauret, N., Cajgfinger, T., Gregoire, T., Grau, E., Feret, J.B., Lopes, M., Guilleux, J., Dedieu, G., Malenovskỳ, Z., Cook, B.D., Morton, D., Rubio, J., Durrieu, S., Cazanave, G., Martin, E., Ristorcelli, T., 2015. Discrete anisotropic radiative transfer (DART 5) for modeling airborne and satellite spectroradiometer and LIDAR acquisitions of natural and urban landscapes. Remote Sens. 7, 1667–1701. https://doi.org/10.3390/rs70201667.

Gui, X., Lian, J., Zhang, R., Li, Y., Shen, H., Ni, Y., Ye, W., 2019. Vertical structure and its biodiversity in a subtropical evergreen broad-leaved forest at Dinghushan in Guangdong Province, China. Biodivers. Sci. 27, 619.

Guillén-Escribà, C., Schneider, F.D., Schmid, B., Tedder, A., Morsdorf, F., Furrer, R., Hueni, A., Niklaus, P.A., Schaepman, M.E., 2021. Remotely sensed between-individual functional trait variation in a temperate forest. Ecol. Evol. 11, 10834–10867. https://doi.org/10.1002/ece3.7758.

Guo, Z., Yan, Z., Majcher, B.M., Lee, C.K.F., Zhao, Y., Song, G., Wang, B., Wang, X., Deng, Y., Michaletz, S.T., Ryu, Y., Ashton, L.A., Lam, H.-M., Wong, M.S., Liu, L., Wu, J., 2022. Dynamic biotic controls of leaf thermoregulation across the diel timescale. Agric. For. Meteorol. 315, 108827 https://doi.org/10.1016/j.agrformet.2022.108827.

Jay, S., Bendoula, R., Hadoux, X., Féret, J.B., Gorretta, N., 2016. A physically-based model for retrieving foliar biochemistry and leaf orientation using close-range imaging spectroscopy. Remote Sens. Environ. 177, 220–236. https://doi.org/10.1016/j.rse.2016.02.029.

Jetz, W., Cavender-Bares, J., Pavlick, R., Schimel, D., Davis, F.W., Asner, G.P., Guralnick, R., Kattge, J., Latimer, A.M., Moorcroft, P., Schaepman, M.E., Schildhauer, M.P., Schneider, F.D., Schrodt, F., Stahl, U., Ustin, S.L., 2016. Monitoring plant functional diversity from space. Nat. Plants 2, 1–5. https://doi.org/10.1038/NPLANTS.2016.24.

Jones, J.B., 2001. Laboratory guide for conducting soil tests and plant analysis. CRC Press.

Kattge, J., Bönisch, G., Díaz, S., Lavorel, S., Prentice, I.C., Leadley, P., Tautenhahn, S., Werner, G.D.A., Aakala, T., Abedi, M., Acosta, A.T.R., Adamidis, G.C., Adamson, K., Aiba, M., Albert, C.H., Alcántara, J.M., Alcázar, C., Aleixo, I., Ali, H., Amiaud, B., Ammer, C., Amoroso, M.M., Anand, M., Anderson, C., Anten, N., Antos, J., Apgaua, D.M.G., Ashman, T.L., Asmara, D.H., Asner, G.P., Aspinwall, M., Atkin, O., Aubin, I., Baastrup-Spohr, L., Bahalkeh, K., Bahn, M., Baker, T., Baker, W.J., Bakker, J.P., Baldocchi, D., Baltzer, J., Banerjee, A., Baranger, A., Barlow, J., Barneche, D.R., Baruch, Z., Bastianelli, D., Battles, J., Bauerle, W., Bauters, M.,

Bazzato, E., Beckmann, M., Beeckman, H., Beierkuhnlein, C., Bekker, R., Belfry, G., Belluau, M., Beloiu, M., Benavides, R., Benomar, L., Berdugo-Lattke, M.L., Berenguer, E., Bergamin, R., Bergmann, J., Bergmann Carlucci, M., Berner, L., Bernhardt-Römermann, M., Bigler, C., Bjorkman, A.D., Blackman, C., Blanco, C., Blonder, B., Blumenthal, D., Bocanegra-González, K.T., Boeckx, P., Bohlman, S., Böhning-Gaese, K., Boisvert-Marsh, L., Bond, W., Bond-Lamberty, B., Boom, A., Boonman, C.C.F., Bordin, K., Boughton, E.H., Boukili, V., Bowman, D.M.J.S., Bravo, S., Brendel, M.R., Broadley, M.R., Brown, K.A., Bruelheide, H., Brumnich, F., Bruun, H.H., Bruy, D., Buchanan, S.W., Bucher, S.F., Buchmann, N., Buitenwerf, R., Bunker, D.E., Bürger, J., Burrascano, S., Burslem, D.F.R.P., Butterfield, B.J., Byun, C., Marques, M., Scalon, M.C., Caccianiga, M., Cadotte, M., Cailleret, M., Camac, J., Camarero, J.J., Campany, C., Campetella, G., Campos, J.A., Cano-Arboleda, L., Canullo, R., Carbognani, M., Carvalho, F., Casanoves, F., Castagneyrol, B., Catford, J. A., Cavender-Bares, J., Cerabolini, B.E.L., Cervellini, M., Chacón-Madrigal, E., Chapin, K., Chapin, F.S., Chelli, S., Chen, S.C., Chen, A., Cherubini, P., Chianucci, F., Choat, B., Chung, K.S., Chytrý, M., Ciccarelli, D., Coll, L., Collins, C.G., Conti, L., Coomes, D., Cornelissen, J.H.C., Cornwell, W.K., Corona, P., Coyea, M., Craine, J., Craven, D., Cromsigt, J.P.G.M., Csecserits, A., Cufar, K., Cuntz, M., da Silva, A.C., Dahlin, K.M., Dainese, M., Dalke, I., Dalle Fratte, M., Dang-Le, A.T., Danihelka, J., Dannoura, M., Dawson, S., de Beer, A.J., De Frutos, A., De Long, J.R., Dechant, B., Delagrange, S., Delpierre, N., Derroire, G., Dias, A.S., Diaz-Toribio, M.H., Dimitrakopoulos, P.G., Dobrowolski, M., Doktor, D., Dřevojan, P., Dong, N., Dransfield, J., Dressler, S., Duarte, L., Ducouret, E., Dullinger, S., Durka, W., Duursma, R., Dymova, O., Eckstein, R.L., Ejtehadi, H., Elser, J., Emilio, T., Engemann, K., Erfanian, M.B., Erfmeier, A., Esquivel-Muelbert, A., Esser, G., Estiarte, M., Domingues, T.F., Fagan, W.F., Fagúndez, J., Falster, D.S., Fan, Y., Fang, J., Farris, E., Fazlioglu, F., Feng, Y., Fernandez-Mendez, F., Ferrara, C., Ferreira, J., Fidelis, A., Finegan, B., Firn, J., Flowers, T.J., Flynn, D.F.B., Fontana, V., Forey, E., Forgiarini, C., François, L., Frangipani, M., Frank, D., Frenette-Dussault, C., Freschet, G.T., Fry, E.L., Fyllas, N.M., Mazzochini, G.G., Gachet, S., Gallagher, R., Ganade, G., Ganga, F., García-Palacios, P., Gargaglione, V., Garnier, E., Garrido, J.L., de Gasper, A.L., Gea-Izquierdo, G., Gibson, D., Gillison, A. N., Giroldo, A., Glasenhardt, M.C., Gleason, S., Gliesch, M., Goldberg, E., Göldel, B., Gonzalez-Akre, E., Gonzalez-Andujar, J.L., González-Melo, A., González-Robles, A., Graae, B.J., Granda, E., Graves, S., Green, W.A., Gregor, T., Gross, N., Guerin, G.R., Günther, A., Gutiérrez, A.G., Haddock, L., Haines, A., Hall, J., Hambuckers, A., Han, W., Harrison, S.P., Hattingh, W., Hawes, J.E., He, T., He, P., Heberling, J.M., Helm, A., Hempel, S., Hentschel, J., Hérault, B., Hereş, A.M., Herz, K., Heuertz, M., Hickler, T., Hietz, P., Higuchi, P., Hipp, A.L., Hirons, A., Hock, M., Hogan, J.A., Holl, K., Honnay, O., Hornstein, D., Hou, E., Hough-Snee, N., Hovstad, K.A., Ichie, T., Igić, B., Illa, E., Isaac, M., Ishihara, M., Ivanov, L., Ivanova, L., Iversen, C.M., Izquierdo, J., Jackson, R.B., Jackson, B., Jactel, H., Jagodzinski, A.M., Jandt, U., Jansen, S., Jenkins, T., Jentsch, A., Jespersen, J.R.P., Jiang, G.F., Johansen, J.L., Johnson, D., Jokela, E.J., Joly, C.A., Jordan, G.J., Joseph, G.S., Junaedi, D., Junker, R.R., Justes, E., Kabzems, R., Kane, J., Kaplan, Z., Kattenborn, T., Kavelenova, L., Kearsley, E., Kempel, A., Kenzo, T., Kerkhoff, A., Khalil, M.I., Kinlock, N.L., Kissling, W.D., Kitajima, K., Kitzberger, T., Kjøller, R., Klein, T., Kleyer, M., Klimešová, J., Klipel, J., Kloeppel, B., Klotz, S., Knops, J.M.H., Kohyama, T., Koike, F., Kollmann, J., Komac, B., Komatsu, K., König, C., Kraft, N.J. B., Kramer, K., Kreft, H., Kühn, I., Kumarathunge, D., Kuppler, J., Kurokawa, H., Kurosawa, Y., Kuyah, S., Laclau, J.P., Lafleur, B., Lallai, E., Lamb, E., Lamprecht, A., Larkin, D.J., Laughlin, D., Le Bagousse-Pinguet, Y., le Maire, G., le Roux, P.C., le Roux, E., Lee, T., Lens, F., Lewis, S.L., Lhotsky, B., Li, Y., Li, X., Lichstein, J.W., Liebergesell, M., Lim, J.Y., Lin, Y.S., Linares, J.C., Liu, C., Liu, D., Liu, U., Livingstone, S., Llusià, J., Lohbeck, M., López-García, Á., Lopez-Gonzalez, G., Lososová, Z., Louault, F., Lukács, B.A., Lukeš, P., Luo, Y., Lussu, M., Ma, S., Maciel Rabelo Pereira, C., Mack, M., Maire, V., Mäkelä, A., Mäkinen, H., Malhado, A.C.M., Mallik, A., Manning, P., Manzoni, S., Marchetti, Z., Marchino, L., Marcilio-Silva, V., Marcon, E., Marignani, M., Markesteijn, L., Martin, A., Martínez-Garza, C., Martínez-Vilalta, J., Mašková, T., Mason, K., Mason, N., Massad, T.J., Masse, J., Mayrose, I., McCarthy, J., McCormack, M.L., McCulloh, K., McFadden, I.R., McGill, B.J., McPartland, M.Y., Medeiros, J.S., Medlyn, B., Meerts, P., Mehrabi, Z., Meir, P., Melo, F.P.L., Mencuccini, M., Meredieu, C., Messier, J., Mészáros, I., Metsaranta, J., Michaletz, S.T., Michelaki, C., Migalina, S., Milla, R., Miller, J.E.D., Minden, V., Ming, R., Mokany, K., Moles, A.T., Molnár, A., Molofsky, J., Molz, M., Montgomery, R.A., Monty, A., Moravcová, L., Moreno-Martínez, A., Moretti, M., Mori, A.S., Mori, S., Morris, D., Morrison, J., Mucina, L., Mueller, S., Muir, C.D., Müller, S.C., Munoz, F., Myers-Smith, I.H., Myster, R.W., Nagano, M., Naidu, S., Narayanan, A., Natesan, B., Negoita, L., Nelson, A.S., Neuschulz, E.L., Ni, J., Niedrist, G., Nieto, J., Niinemets, Ü., Nolan, R., Nottebrock, H., Nouvellon, Y., Novakovskiy, A., Nystuen, K.O., O'Grady, A., O'Hara, K., O'Reilly-Nugent, A., Oakley, S., Oberhuber, W., Ohtsuka, T., Oliveira, R., Öllerer, K., Olson, M.E., Onipchenko, V., Onoda, Y., Onstein, R.E., Ordonez, J.C., Osada, N., Ostonen, I., Ottaviani, G., Otto, S., Overbeck, G.E., Ozinga, W.A., Pahl, A.T., Paine, C.E.T., Pakeman, R.J., Papageorgiou, A.C., Parfionova, E., Pärtel, M., Patacca, M., Paula, S., Paule, J., Pauli, H., Pausas, J.G., Peco, B., Penuelas, J., Perea, A., Peri, P.L., Petisco-Souza, A.C., Petraglia, A., Petritan, A.M., Phillips, O.L., Pierce, S., Pillar, V.D., Pisek, J., Pomogaybin, A., Poorter, H., Portsmuth, A., Poschlod, P., Potvin, C., Pounds, D., Powell, A.S., Power, S.A., Prinzing, A., Puglielli, G., Pyšek, P., Raevel, V., Rammig, A., Ransijn, J., Ray, C.A., Reich, P.B., Reichstein, M., Reid, D.E.B., Réjou-Méchain, M., de Dios, V.R., Ribeiro, S., Richardson, S., Riibak, K., Rillig, M.C., Riviera, F., Robert, E.M.R., Roberts, S., Robroek, B., Roddy, A., Rodrigues, A.V., Rogers, A., Rollinson, E., Rolo, V., Römermann, C., Ronzhina, D., Roscher, C., Rosell, J.A., Rosenfield, M.F., Rossi, C., Roy, D.B., Royer-Tardif, S., Rüger, N., Ruiz-Peinado, R., Rumpf, S.B., Rusch, G.M., Ryo, M., Sack, L., Saldaña, A., Salgado-Negret, B., Salguero-Gomez, R., Santa-Regina, I., Santacruz-García, A.C., Santos, J., Sardans, J., Schamp, B., Scherer-Lorenzen, M., Schleuning, M., Schmid, B., Schmidt, M., Schmitt, S., Schneider, J.V., Schowanek, S.D., Schrader, J., Schrodt, F., Schuldt, B., Schurr, F., Selaya Garvizu, G., Semchenko, M., Seymour, C., Sfair, J.C., Sharpe, J.M., Sheppard, C.S., Sheremetiev, S., Shiodera, S., Shipley, B., Shovon, T.A., Siebenkäs, A., Sierra, C., Silva, V., Silva, M., Sitzia, T., Sjöman, H., Slot, M., Smith, N. G., Sodhi, D., Soltis, P., Soltis, D., Somers, B., Sonnier, G., Sørensen, M.V., Sosinski, E. E., Soudzilovskaia, N.A., Souza, A.F., Spasojevic, M., Sperandii, M.G., Stan, A.B., Stegen, J., Steinbauer, K., Stephan, J.G., Sterck, F., Stojanovic, D.B., Strydom, T., Suarez, M.L., Svenning, J.C., Svitková, I., Svitok, M., Svoboda, M., Swaine, E., Swenson, N., Tabarelli, M., Takagi, K., Tappeiner, U., Tarifa, R., Tauugourdeau, S., Tavsanoglu, C., te Beest, M., Tedersoo, L., Thiffault, N., Thom, D., Thomas, E., Thompson, K., Thornton, P.E., Thuiller, W., Tichý, L., Tissue, D., Tjoelker, M.G., Tng, D.Y.P., Tobias, J., Török, P., Tarin, T., Torres-Ruiz, J.M., Tóthmérész, B., Treurnicht, M., Trivellone, V., Trolliet, F., Trotsiuk, V., Tsakalos, J.L., Tsiripidis, I., Tysklind, N., Umehara, T., Usoltsev, V., Vadeboncoeur, M., Vaezi, J., Valladares, F., Vamosi, J., van Bodegom, P.M., van Breugel, M., Van Cleemput, E., van de Weg, M., van der Merwe, S., van der Plas, F., van der Sande, M.T., van Kleunen, M., Van Meerbeek, K., Vanderwel, M., Vanselow, K.A., Vårhammar, A., Varone, L., Vasquez Valderrama, M.Y., Vassilev, K., Vellend, M., Veneklaas, E.J., Verbeeck, H., Verheyen, K., Vibrans, A., Vieira, I., Villacís, J., Violle, C., Vivek, P., Wagner, K., Waldram, M., Waldron, A., Walker, A.P., Waller, M., Walther, G., Wang, H., Wang, F., Wang, W., Watkins, H., Watkins, J., Weber, U., Weedon, J.T., Wei, L., Weigelt, P., Weiher, E., Wells, A.W., Wellstein, C., Wenk, E., Westoby, M., Westwood, A., White, P.J., Whitten, M., Williams, M., Winkler, D.E., Winter, K., Womack, C., Wright, I.J., Wright, S.J., Wright, J., Pinho, B.X., Ximenes, F., Yamada, T., Yamaji, K., Yanai, R., Yankov, N., Yguel, B., Zanini, K.J., Zanne, A.E., Zelený, D., Zhao, Y.P., Zheng, Jingming, Ji, Ziemińska, Zirbel, C.R., Zizka, G., Zo-Bi, I.C., Zotz, G., Wirth, C., 2020. TRY plant trait database – enhanced coverage and open access. Glob. Change Biol. 26, 119–188. https://doi.org/10.1111/gcb.14904.

Kattenborn, T., Schiefer, F., Zarco-Tejada, P., Schmidtlein, S., 2019. Advantages of retrieving pigment content [μg/cm2] versus concentration [%] from canopy reflectance. Remote Sens. Environ. 230, 111195 https://doi.org/10.1016/j.rse.2019.05.014.

Kattge, J., Knorr, W., Raddatz, T., Wirth, C., 2009. Quantifying photosynthetic capacity and its relationship to leaf nitrogen content for global-scale terrestrial biosphere models. Glob. Change Biol. 15, 976–991. https://doi.org/10.1111/j.1365-2486.2008.01744.x.

Knyazikhin, Y., Schull, M.A., Stenberg, P., Mõttus, M., Rautiainen, M., Yang, Y., Marshak, A., Carmona, P.L., Kaufmann, R.K., Lewis, P., Disney, M.I., Vanderbilt, V., Davis, A.B., Baret, F., Jacquemoud, S., Lyapustin, A., Myneni, R.B., 2013. Hyperspectral remote sensing of foliar nitrogen content. Proc. Natl. Acad. Sci. U. S. A. 110, 1–8. https://doi.org/10.1073/pnas.1210196109.

Kobayashi, H., Baldocchi, D.D., Ryu, Y., Chen, Q., Ma, S., Osuna, J.L., Ustin, S.L., 2012. Modeling energy and carbon fluxes in a heterogeneous oak woodland: a three-dimensional approach. Agric. For. Meteorol. 152, 83–100. https://doi.org/10.1016/j.agrformet.2011.09.008.

Kokaly, R.F., Asner, G.P., Ollinger, S.V., Martin, M.E., Wessman, C.A., 2009. Characterizing canopy biochemistry from imaging spectroscopy and its application to ecosystem studies. Remote Sens. Environ. 113, S78–S91. https://doi.org/10.1016/j.rse.2008.10.018.

Kumagai, E., Burroughs, C.H., Pederson, T.L., Montes, C.M., Peng, B., Kimm, H., Guan, K., Ainsworth, E.A., Bernacchi, C.J., 2021. Predicting biochemical acclimation of leaf photosynthesis in soybean under in-field canopy warming using hyperspectral reflectance. Plant Cell Environ. 1–15 https://doi.org/10.1111/pce.14204.

Kupiec, J.A., Curran, P.J., 1995. Decoupling effects of the canopy and foliar biochemicals in AVIRIS spectra. Int. J. Remote Sens. 16, 1731–1739. https://doi.org/10.1080/01431169508954510.

Lamour, J., Davidson, K.J., Ely, K.S., Anderson, J.A., Rogers, A., Wu, J., Serbin, S.P., 2021. Rapid estimation of photosynthetic leaf traits of tropical plants in diverse environmental conditions using reflectance spectroscopy. Plos One 16, e0258791. https://doi.org/10.1371/journal.pone.0258791.

le Maire, G., François, C., Soudani, K., Berveiller, D., Pontailler, J.-Y., Bréda, N., Genet, H., Davi, H., Dufrêne, E., 2008. Calibration and validation of hyperspectral indices for the estimation of broadleaved forest leaf chlorophyll content, leaf mass per area, leaf area index and leaf canopy biomass. Remote Sens. Environ. 112, 3846–3864. https://doi.org/10.1016/j.rse.2008.06.005.

Long, S.P., 2003. Gas exchange measurements, what can they tell us about the underlying limitations to photosynthesis? Procedures and sources of error. J. Exp. Bot. 54, 2393–2401. https://doi.org/10.1093/jxb/erg262.

Martin, M.E., Plourde, L.C., Ollinger, S.V., Smith, M.L., McNeil, B.E., 2008. A generalizable method for remote sensing of canopy nitrogen across a wide range of forest ecosystems. Remote Sens. Environ. 112, 3511–3519. https://doi.org/10.1016/j.rse.2008.04.008.

Martin, R.E., Dana Chadwick, K., Brodrick, P.G., Carranza-Jimenez, L., Vaughn, N.R., Asner, G.P., 2018. An approach for foliar trait retrieval from airborne imaging spectroscopy of tropical forests. Remote Sens. 10 https://doi.org/10.3390/rs10020199.

Meacham-Hensold, K., Fu, P., Wu, J., Serbin, S., Montes, C.M., Ainsworth, E., Guan, K., Dracup, E., Pederson, T., Driever, S., Bernacchi, C., 2020. Plot-level rapid screening for photosynthetic parameters using proximal hyperspectral imaging. J. Exp. Bot. 71, 2312–2328. https://doi.org/10.1093/jxb/eraa068.

Mengoli, G., Agustí-Panareda, A., Boussetta, S., Harrison, S.P., Trotta, C., Prentice, I.C., 2022. Ecosystem photosynthesis in land-surface models: a first-principles approach incorporating acclimation. J. Adv. Model. Earth Syst. 14, e2021MS002767 https://doi.org/10.1029/2021MS002767.

Nakaji, T., Oguma, H., Nakamura, M., Kachina, P., Asanok, L., Marod, D., Aiba, M., Kurokawa, H., Kosugi, Y., Kassim, A.R., Hiura, T., 2019. Estimation of six leaf traits of east asian forest tree species by leaf spectroscopy and partial least square regression. Remote Sens. Environ. 233, 111381 https://doi.org/10.1016/j.rse.2019.111381.

Ollinger, S.V., 2011. Sources of variability in canopy reflectance and the convergent properties of plants. New Phytol. 189, 375–394. https://doi.org/10.1111/j.1469-8137.2010.03536.x.

Osnas, J.L.D., Lichstein, J.W., Reich, P.B., Pacala, S.W., 2013. Global leaf trait relationships: mass, area, and the leaf economics spectrum. Science 340, 741–744. https://doi.org/10.1126/science.1231574.

Pedregosa, F., Varoquaux, G., Gramfort, A., Michel, V., Thirion, B., Grisel, O., Blondel, M., Prettenhofer, P., Weiss, R., Dubourg, V., Vanderplas, J., Passos, A., Cournapeau, D., Brucher, M., Perrot, M., Duchesnay, É., 2011. Scikit-learn: machine learning in python. J. Mach. Learn. Res. 12, 2825–2830.

Ricciuto, D., Sargsyan, K., Thornton, P., 2018. The impact of parametric uncertainties on biogeochemistry in the E3SM land model. J. Adv. Model. Earth Syst. 10, 297–319. https://doi.org/10.1002/2017MS000962.

Richards, J.A., 2013. Remote Sensing Digital Image Analysis. Springer Berlin Heidelberg, Berlin, Heidelberg. https://doi.org/10.1007/978-3-642-30062-2.

Roberts, D.A., Ustin, S.L., Ogunjemiyo, S., Greenberg, J., Dobrowski, S.Z., Chen, J., Hinckley, T.M., 2004. Spectral and structural measures of northwest Forest vegetation at leaf to landscape scales. Ecosystems 7. https://doi.org/10.1007/s10021-004-0144-5.

Rogers, A., 2014. The use and misuse of vc, max in earth system models. Photosynth. Res. 119, 15–29. https://doi.org/10.1007/s11120-013-9818-1.

Rogers, A., Medlyn, B.E., Dukes, J.S., Bonan, G., von Caemmerer, S., Dietze, M.C., Kattge, J., Leakey, A.D.B., Mercado, L.M., Niinemets, Ü., Prentice, I.C., Serbin, S.P., Sitch, S., Way, D.A., Zaehle, S., 2017. A roadmap for improving the representation of photosynthesis in earth system models. New Phytol. 213, 22–42. https://doi.org/10.1111/nph.14283.

Ryu, Y., Berry, J.A., Baldocchi, D.D., 2019. What is global photosynthesis? History, uncertainties and opportunities. Remote Sens. Environ. 223, 95–114. https://doi.org/10.1016/j.rse.2019.01.016.

Savitzky, Abraham, Golay, M.J.E., 1964. Smoothing and differentiation of data by simplified least squares procedures. Anal. Chem. 36, 1627–1639. https://doi.org/10.1021/ac60214a047.

Schneider, F.D., Morsdorf, F., Schmid, B., Petchey, O.L., Hueni, A., Schimel, D.S., Schaepman, M.E., 2017. Mapping functional diversity from remotely sensed morphological and physiological forest traits. Nat. Commun. 8 https://doi.org/10.1038/s41467-017-01530-3.

Schweiger, A.K., Cavender-Bares, J., Townsend, P.A., Hobbie, S.E., Madritch, M.D., Wang, R., Tilman, D., Gamon, J.A., 2018. Plant spectral diversity integrates functional and phylogenetic components of biodiversity and predicts ecosystem function. Nat. Ecol. Evol. 2, 976–982. https://doi.org/10.1038/s41559-018-0551-1.

Seabold, S., Perktold, J., 2010. Statsmodels: econometric and statistical modeling with python. In: Presented at the Python in Science Conference, Austin, Texas, pp. 92–96. https://doi.org/10.25080/Majora-92bf1922-011.

Serbin, S.P., Singh, A., Desai, A.R., Dubois, S.G., Jablonski, A.D., Kingdon, C.C., Kruger, E.L., Townsend, P.A., 2015. Remotely estimating photosynthetic capacity, and its response to temperature, in vegetation canopies using imaging spectroscopy. Remote Sens. Environ. 167, 78–87. https://doi.org/10.1016/j.rse.2015.05.024.

Serbin, S.P., Singh, A., McNeil, B.E., Kingdon, C.C., Townsend, P.A., 2014. Spectroscopic determination of leaf morphological and biochemical traits for northern temperate and boreal tree species. Ecol. Appl. 24, 1651–1669. https://doi.org/10.1890/13-2110.1.

Serbin, S.P., Townsend, P.A., 2020. Scaling functional traits from leaves to canopies. Remote Sens. Plant Biodivers. 43–82 https://doi.org/10.1007/978-3-030-33157-3_3.

Serbin, S.P., Wu, J., Ely, K.S., Kruger, E.L., Townsend, P.A., Meng, R., Wolfe, B.T., Chlus, A., Wang, Z., Rogers, A., 2019. From the Arctic to the tropics: multibiome prediction of leaf mass per area using leaf reflectance. New Phytol. 224, 1557–1568. https://doi.org/10.1111/nph.16123.

Serrano, L., Peñuelas, J., Ustin, S.L., 2002. Remote sensing of nitrogen and lignin in Mediterranean vegetation from AVIRIS data: decomposing biochemical from structural signals. Remote Sens. Environ. 81, 355–364. https://doi.org/10.1016/S0034-4257(02)00011-1.

Shen, T., Corlett, R.T., Song, L., Ma, W., Guo, X., Song, Y., Wu, Y., 2018. Vertical gradient in bryophyte diversity and species composition in tropical and subtropical forests in Yunnan, SW China. J. Veg. Sci. 29, 1075–1087.

Shiklomanov, A.N., Dietze, M.C., Viskari, T., Townsend, P.A., Serbin, S.P., 2016. Quantifying the influences of spectral resolution on uncertainty in leaf trait estimates through a bayesian approach to RTM inversion. Remote Sens. Environ. 183, 226–238. https://doi.org/10.1016/j.rse.2016.05.023.

Shiklomanov, A.N., Dietze, M.C., Fer, I., Viskari, T., Serbin, S.P., 2021. Cutting out the middleman: calibrating and validating a dynamic vegetation model (ED2-PROSPECT5) using remotely sensed surface reflectance. Geosci. Model Dev. 14, 2603–2633. https://doi.org/10.5194/gmd-14-2603-2021.

Silva-Perez, V., Molero, G., Serbin, S.P., Condon, A.G., Reynolds, M.P., Furbank, R.T., Evans, J.R., 2018. Hyperspectral reflectance as a tool to measure biochemical and physiological traits in wheat. J. Exp. Bot. 69, 483–496. https://doi.org/10.1093/jxb/erx421.

Singh, A., Serbin, S.P., McNeil, B.E., Kingdon, C.C., Townsend, P.A., 2015. Imaging spectroscopy algorithms for mapping canopy foliar chemical and morphological traits and their uncertainties. Ecol. Appl. 25, 2180–2197. https://doi.org/10.1890/14-2098.1.

Sinha, S.K., Padalia, H., Dasgupta, A., Verrelst, J., Rivera, J.P., 2020. Estimation of leaf area index using PROSAIL based LUT inversion, MLRA-GPR and empirical models: case study of tropical deciduous forest plantation, North India. Int. J. Appl. Earth Obs. Geoinf. 86, 102027 https://doi.org/10.1016/j.jag.2019.102027.

Smith, N.G., Dukes, J.S., 2018. Drivers of leaf carbon exchange capacity across biomes at the continental scale. Ecology 99, 1610–1620. https://doi.org/10.1002/ecy.2370.

Stinziano, J.R., Morgan, P.B., Lynch, D.J., Saathoff, A.J., McDermitt, D.K., Hanson, D.T., 2017. The rapid A-ci response: photosynthesis in the phenomic era. Plant Cell Environ. 40, 1256–1262. https://doi.org/10.1111/pce.12911.

Stovall, A.E.L., Masters, B., Fatoyinbo, L., Yang, X., 2021. TLSLeAF: automatic leaf angle estimates from single-scan terrestrial laser scanning. New Phytol. 232, 1876–1892. https://doi.org/10.1111/nph.17548.

Tagliabue, G., Boschetti, M., Bramati, G., Candiani, G., Colombo, R., Nutini, F., Pompilio, L., Rivera-Caicedo, J.P., Rossi, M., Rossini, M., Verrelst, J., Panigada, C., 2022. Hybrid retrieval of crop traits from multi-temporal PRISMA hyperspectral imagery. ISPRS J. Photogramm. Remote Sens. 187, 362–377. https://doi.org/10.1016/j.isprsjprs.2022.03.014.

Thomson, E.R., Spiegel, M.P., Althuizen, I.H.J., Bass, P., Chen, S., Chmurzynski, A., Halbritter, A.H., Henn, J.J., Jónsdóttir, I.S., Klanderud, K., Li, Y., Maitner, B.S., Michaletz, S.T., Niittynen, P., Roos, R.E., Telford, R.J., Enquist, B.J., Vandvik, V., Macias-Fauria, M., Malhi, Y., 2021. Multiscale mapping of plant functional groups and plant traits in the high Arctic using field spectroscopy, UAV imagery and sentinel-2A data. Environ. Res. Lett. 16 https://doi.org/10.1088/1748-9326/abf464.

Timmermans, J., van der Tol, C., Verhoef, W., Vekerdy, Z., van Laake, P., Su, Z., 2008. Intercomparison of SAIL and DART over a pine forest using laserscan derived structural parameters.

Townsend, P.A., Foster, J.R., Chastain, R.A., Currie, W.S., 2003. Application of imaging spectroscopy to mapping canopy nitrogen in the forests of the central Appalachian Mountains using hyperion and AVIRIS. IEEE Trans. Geosci. Remote Sens. 41, 1347–1354.

Uddling, J., Gelang-Alfredsson, J., Piikki, K., Pleijel, H., 2007. Evaluating the relationship between leaf chlorophyll concentration and SPAD-502 chlorophyll meter readings. Photosynth. Res. 91, 37–46. https://doi.org/10.1007/s11120-006-9077-5.

Ustin, S.L., Gitelson, A.A., Jacquemoud, S., Schaepman, M., Asner, G.P., Gamon, J.A., Zarco-Tejada, P., 2009. Retrieval of foliar information about plant pigment systems from high resolution spectroscopy. Remote Sens. Environ. 113, S67–S77. https://doi.org/10.1016/j.rse.2008.10.019.

Verhoef, W., Jia, L., Xiao, Q., Su, Z., 2007. Unified optical-thermal four-stream radiative transfer theory for homogeneous vegetation canopies. IEEE Trans. Geosci. Remote Sens. 45, 1808–1822. https://doi.org/10.1109/TGRS.2007.895844.

Verrelst, J., Rivera, J.P., Gitelson, A., Delegido, J., Moreno, J., Camps-Valls, G., 2016. Spectral band selection for vegetation properties retrieval using gaussian processes regression. Int. J. Appl. Earth Obs. Geoinform. 52, 554–567. https://doi.org/10.1016/j.jag.2016.07.016.

Verrelst, J., Rivera, J.P., van der Tol, C., Magnani, F., Mohammed, G., Moreno, J., 2015. Global sensitivity analysis of the SCOPE model: What drives simulated canopy-leaving sun-induced fluorescence? Remote Sens. Environ. 166, 8–21. https://doi.org/10.1016/j.rse.2015.06.002.

Verrelst, J., Rivera-Caicedo, J.P., Reyes-Muñoz, P., Morata, M., Amin, E., Tagliabue, G., Panigada, C., Hank, T., Berger, K., 2021. Mapping landscape canopy nitrogen content from space using PRISMA data. ISPRS J. Photogramm. Remote Sens. 178, 382–395. https://doi.org/10.1016/j.isprsjprs.2021.06.017.

Vincent, G., Antin, C., Laurans, M., Heurtebize, J., Durrieu, S., Lavalley, C., Dauzat, J., 2017. Mapping plant area index of tropical evergreen forest by airborne laser scanning. A cross-validation study using LAI2200 optical sensor. Remote Sens. Environ. 198, 254–266. https://doi.org/10.1016/j.rse.2017.05.034.

Violle, C., Navas, M.-L., Vile, D., Kazakou, E., Fortunel, C., Hummel, I., Garnier, E., 2007. Let the concept of trait be functional! Oikos 116, 882–892. https://doi.org/10.1111/j.2007.0030-1299.15559.x.

Walker, A.P., Beckerman, A.P., Gu, L., Kattge, J., Cernusak, L.A., Domingues, T.F., Scales, J.C., Wohlfahrt, G., Wullschleger, S.D., Woodward, F.I., 2014. The relationship of leaf photosynthetic traits - vcmax and jmax - to leaf nitrogen, leaf phosphorus, and specific leaf area: a meta-analysis and modeling study. Ecol. Evol. 4, 3218–3235. https://doi.org/10.1002/ece3.1173.

Walker, A.P., De Kauwe, M.G., Bastos, A., Belmecheri, S., Georgiou, K., Keeling, R.F., McMahon, S.M., Medlyn, B.E., Moore, D.J.P., Norby, R.J., Zaehle, S., Anderson-Teixeira, K.J., Battipaglia, G., Brienen, R.J.W., Cabugao, K.G., Cailleret, M., Campbell, E., Canadell, J.G., Ciais, P., Craig, M.E., Ellsworth, D.S., Farquhar, G.D., Fatichi, S., Fisher, J.B., Frank, D.C., Graven, H., Gu, L., Haverd, V., Heilman, K., Heimann, M., Hungate, B.A., Iversen, C.M., Joos, F., Jiang, M., Keenan, T.F., Knauer, J., Körner, C., Leshyk, V.O., Leuzinger, S., Liu, Y., MacBean, N., Malhi, Y., McVicar, T.R., Penuelas, J., Pongratz, J., Powell, A.S., Riutta, T., Sabot, M.E.B., Schleucher, J., Sitch, S., Smith, W.K., Sulman, B., Taylor, B., Terrer, C., Torn, M.S., Treseder, K.K., Trugman, A.T., Trumbore, S.E., van Mantgem, P.J., Voelker, S.L., Whelan, M.E., Zuidema, P.A., 2021. Integrating the evidence for a terrestrial carbon sink caused by increasing atmospheric CO2. New Phytol. 229, 2413–2445. https://doi.org/10.1111/nph.16866.

Wang, Z., Chlus, A., Geygan, R., Ye, Z., Zheng, T., Singh, A., Couture, J.J., Cavender-Bares, J., Kruger, E.L., Townsend, P.A., 2020. Foliar functional traits from imaging spectroscopy across biomes in eastern North America. New Phytol. 228, 494–511. https://doi.org/10.1111/nph.16711.

Wang, Z., Skidmore, A.K., Wang, T., Darvishzadeh, R., Heiden, U., Heurich, M., Latifi, H., Hearne, J., 2017. Canopy foliar nitrogen retrieved from airborne hyperspectral

imagery by correcting for canopy structure effects. Int. J. Appl. Earth Obs. Geoinform. 54, 84–94. https://doi.org/10.1016/j.jag.2016.09.008.
Wang, Z., Townsend, P.A., Kruger, E.L., 2022. Leaf spectroscopy reveals divergent inter- and intra-species foliar trait covariation and trait–environment relationships across NEON domains. New Phytol. 235, 923–938. https://doi.org/10.1111/nph.18204.
Wessman, C.A., Aber, J.D., Peterson, D.L., Melillo, J.M., 1988. Remote sensing of canopy chemistry and nitrogen cycling in temperate forest ecosystems. Nature 335, 154–156. https://doi.org/10.1038/335154a0.
Wieczynski, D.J., Díaz, S., Durán, S.M., Fyllas, N.M., Salinas, N., Martin, R.E., Shenkin, A., Silman, M.R., Asner, G.P., Bentley, L.P., Malhi, Y., Enquist, B.J., Savage, V.M., 2022. Improving landscape-scale productivity estimates by integrating trait-based models and remotely-sensed foliar-trait and canopy-structural data. Ecography e06078. https://doi.org/10.1111/ecog.06078.
Wold, S., Sjöström, M., Eriksson, L., 2001. PLS-regression: a basic tool of chemometrics. Chemom. Intell. Lab. Syst. 58, 109–130. https://doi.org/10.1016/S0169-7439(01)00155-1.
Wright, I.J., Reich, P.B., Westoby, M., Ackerly, D.D., Baruch, Z., Bongers, F., Cavender-Bares, J., Chapin, T., Cornellssen, J.H.C., Diemer, M., Flexas, J., Garnier, E., Groom, P.K., Gulias, J., Hikosaka, K., Lamont, B.B., Lee, T., Lee, W., Lusk, C., Midgley, J.J., Navas, M.L., Niinemets, Ü., Oleksyn, J., Osada, H., Poorter, H., Pool, P., Prior, L., Pyankov, V.I., Roumet, C., Thomas, S.C., Tjoelker, M.G., Veneklaas, E.J., Villar, R., 2004. The worldwide leaf economics spectrum. Nature 428. https://doi.org/10.1038/nature02403.
Wu, J., Kobayashi, H., Stark, S.C., Meng, R., Guan, K., Tran, N.N., Gao, S., Yang, W., Restrepo-coupe, N., Miura, T., Oliviera, R.C., Rogers, A., Dye, D.G., Nelson, B.W., Serbin, S.P., Huete, A.R., Saleska, S.R., 2018. Biological processes dominate seasonality of remotely sensed canopy greenness in an Amazon evergreen forest. New Phytol. 217, 1507–1520. https://doi.org/10.1111/nph.14939.
Wu, J., Rogers, A., Albert, L.P., Ely, K., Prohaska, N., Wolfe, B.T., Oliveira, R.C., Saleska, S.R., Serbin, S.P., 2019. Leaf reflectance spectroscopy captures variation in carboxylation capacity across species, canopy environment and leaf age in lowland moist tropical forests. New Phytol. 224, 663–674. https://doi.org/10.1111/nph.16029.
Yan, Z., Guo, Z., Serbin, S.P., Song, G., Zhao, Y., Chen, Y., Wu, S., Wang, J., Wang, X., Li, J., Wang, B., Wu, Y., Su, Y., Wang, H., Rogers, A., Liu, L., Wu, J., 2021. Spectroscopy outperforms leaf trait relationships for predicting photosynthetic capacity across different forest types. New Phytol. 232, 134–147. https://doi.org/10.1111/nph.17579.
Ye, W.H., Cao, H.L., Huang, Z.L., Lian, J.Y., Wang, Z.G., Li, L., Wei, S.G., Wang, Z.M., 2008. Community structure of a 20 hm2 lower subtropical evergreen broadleaved forest plot in Dinghushan, China. Chin. J. Plant Ecol. 32, 274.
Yi, X., Wang, N., Ren, H., Yu, J., Hu, T., Su, Y., Mi, X., Guo, Q., Ma, K., 2022. From canopy complementarity to asymmetric competition: the negative relationship between structural diversity and productivity during succession. J. Ecol. 110, 457–465. https://doi.org/10.1111/1365-2745.13813.
Zeng, Y., Hao, D., Huete, A., Dechant, B., Berry, J., Chen, J.M., Joiner, J., Frankenberg, C., Bond-Lamberty, B., Ryu, Y., Xiao, J., Asrar, G.R., Chen, M., 2022. Optical vegetation indices for monitoring terrestrial ecosystems globally. Nat. Rev. Earth Environ. 1–17 https://doi.org/10.1038/s43017-022-00298-5.
Zhao, Y., Zeng, Y., Zheng, Z., Dong, W., Zhao, D., Wu, B., Zhao, Q., 2018. Forest species diversity mapping using airborne LiDAR and hyperspectral data in a subtropical forest in China. Remote Sens. Environ. 213, 104–114. https://doi.org/10.1016/j.rse.2018.05.014.
Zheng, Z., Zeng, Y., Schneider, F.D., Zhao, Y., Zhao, D., Schmid, B., Schaepman, M.E., Morsdorf, F., 2021. Mapping functional diversity using individual tree-based morphological and physiological traits in a subtropical forest. Remote Sens. Environ. 252, 112170 https://doi.org/10.1016/j.rse.2020.112170.
Zou, J., Yan, G., Zhu, L., Zhang, W., 2009. Woody-to-total area ratio determination with a multispectral canopy imager. Tree Physiol. 29, 1069–1080. https://doi.org/10.1093/treephys/tpp042.